Synthesis and Characterization of Molecule-Based Magnets Containing Methyl-Substituted Phenyltricyanoethylene Acceptors

James Arnold King, Jr.

Thesis submitted to the faculty of the Virginia Polytechnic Institute and State University in partial fulfillment of the requirements for the degree of

Master of Science

In

Chemistry

Gordon Yee, Committee Chair

Paul Deck, Committee Member

Brian Hanson, Committee Member

September 1, 2009

Blacksburg, Virginia

Keywords: molecule-based magnets, ordering temperature, ferrimagnet

Synthesis and Characterization of Molecule-Based Magnets Containing Methyl-Substituted Phenyltricyanoethylene Acceptors

James Arnold King, Jr.

ABSTRACT

A new family of molecule-based magnets related to the $V[PTCE]_x \cdot yCH_2Cl_2$ magnet (PTCE = phenyltricyanoethylene, x = ~2, y = ~0.2) was synthesized utilizing new reversible one-electron acceptors with the general form Me_xPTCE (PTCE = phenyltricyanoethylene, x is the number of methyl groups on the phenyl ring, Me = $-CH_3$). These new acceptors were synthesized for the purpose of studying electronic and steric effects of the substitution of the phenyl ring with electron donating groups on the overall magnetic properties of the solid, specifically to contrast their behavior with materials that contain similar trifluoromethyl ($-CF_3$) substituted acceptors. These electron-poor olefins react with $V(CO)_6$ in dichloromethane (CH_2Cl_2) under N_2 to yield air-sensitive, amorphous magnetic coordination polymers that exhibit ordering temperatures ranging from 160 K to 250 K and display anhysteretic behavior at all temperatures. The magnets synthesized in this project were all characterized and studied using magnetic measurements, infrared spectroscopy, and elemental analysis. The neutral acceptors used were characterized using NMR spectroscopy, infrared spectroscopy, mass spectrometry, cyclic voltammetry, and modeled using density functional theory (DFT) calculations.

Table of Contents

1. Magnetism: Background and Measurement

1.1 Background

Magnetism has been one of the least understood of the natural forces, and scientists have attempted to study this phenomenon for centuries. When charged particles accelerate, they produce magnetic fields. These magnetic fields vary in size from microscopic fields created by the spin and orbital motions of an electron within certain atoms or ions to macroscopic fields that result from an electric current that moves within a conductor or the north and south poles of a bar magnet. Advances in the study of magnetism have led to the implementation of new materials in a variety of applications such as data storage (1) and magnetic resonance imaging (MRI) contrast agents (2).

Magnetic materials are present in everyday applications, from loudspeakers to recording media to electromagnets, with the details of the application determining what material is used. Miniaturization (such as computers and cellular phones) drives the field of magnetic materials towards one of huge interest and demand (3).

Atom-based magnets (magnets that have only spins on d or f type orbitals on metal ions or atoms contributing to the overall spin state) have dominated magnetic materials for centuries (4), but certain applications such as memory storage in computers are beginning to require materials where the physical and magnetic properties are more finely controlled (5). There is not a great deal of electronic tunability involved with atom-based magnets (6), other than percent composition, so efforts have shifted to studying molecules, as opposed to atoms, as building blocks for magnetic materials. The study of magnets derived from organic molecules has been

of particular interest to chemists and physicists for nearly two decades due to the possible applications for which they could be utilized, such as spintronics, or the implementation of electron spins and their magnetic moments in devices (7). Using the molecule-based magnet families developed in the 80's and 90's, scientists today can explore new avenues by varying the components of those magnets.

1.1.1 Electron Magnetic Moments

The magnetic properties of any material depend on the orbital and spin motions of the electrons within the atoms and molecules, as well as those electrons' interactions among one another. An unpaired electron in an atom or ion can generate a magnetic field based on orbital contribution (movement about the nucleus) and spin contribution (spin orientation within the orbital), which are represented by Equations 1 and 2, respectively:

$$\boldsymbol{m}_0 = -\left(\frac{e}{2m_e}\right)\boldsymbol{p}_0 \qquad (1)$$

$$\boldsymbol{m}_s = -\frac{e\boldsymbol{p}_s}{m_e} \qquad (2)$$

In Eq. 1-2, $\boldsymbol{m}_o$ is the orbital magnetic moment, $\boldsymbol{m}_s$ is the spin magnetic moment, e is the charge on the electron, m_e is the mass of the electron, $\boldsymbol{p}_o$ is the orbital angular momentum, and $\boldsymbol{p}_s$ is the spin angular momentum. The overall sum of these interactions determines the magnetic behavior of an electron, so the above equations can be vector-summed to arrive at Equation 3:

$$\boldsymbol{m}_{\text{tot}} = \boldsymbol{m}_0 + \boldsymbol{m}_s = -g\left(\frac{e}{2m_e}\right)\boldsymbol{p}_{tot} \qquad (3)$$

In Eq. 3, $\boldsymbol{p}_{\text{tot}}$ is the total angular momentum of the electron and g is a constant known as the Lande splitting factor, or g-factor. The value of the g-factor is 2.002319 for a free electron, but differs based on the chemical system involved.

1.1.2 Diamagnetism and Paramagnetism

All substance can be assigned to one of two main classes, depending on the electron configuration of the species. If there are no unpaired electrons present in the electronic structure, that species is said to be diamagnetic. The individual spin of any particular electron in an orbital is counteracted by the electron with which it is paired, and no net moment is observed. When exposed to an applied magnetic field, diamagnetic materials are slightly repelled by the field. When a species contains any number of unpaired electrons within its electronic structure, it is considered to be paramagnetic, and is attracted to an applied field. Examples of paramagnetic materials include atoms and ions such as Cu^0 (1 unpaired e^-) and V^{3+} (2 unpaired e^-), and molecules and complexes such as O_2 (2 unpaired e^-) and $V(CO)_6$ (1 unpaired e^-).

1.1.3 Magnetization

Eq. 3 describes the magnetic moment of an individual electron, but in bulk solids, the magnetization, *M* is utilized. The term magnetization is described as the magnetic moment over a volume of space. If the individual magnetic moments in a certain volume of space can be thought of as vector quantities, the magnetization is the vector sum of all the moments within that volume.

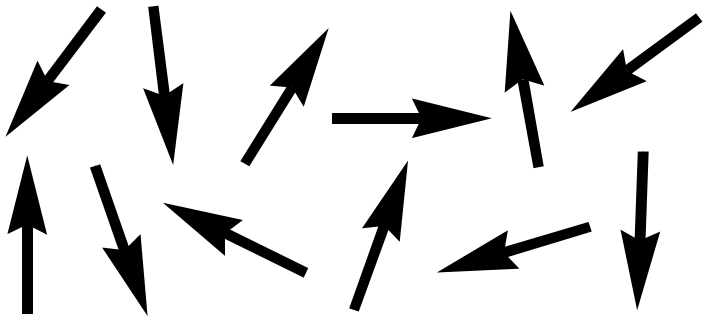

Figure 1. Individual moments are randomly oriented and essentially have no influence over one another, characteristic of a paramagnet.

1.2 Ordering Phenomena

1.2.1 Exchange Interactions

Magnetic exchange interactions, which govern communication between unpaired electrons, are the key to understanding the properties of magnetic materials. The four exchange interactions are direct exchange, superexchange, indirect exchange, and itinerant exchange (8), but for the purposes of this project, only direct exchange and superexchange will be discussed in detail, as indirect and itinerant exchange are not relevant in molecule-based magnets. Exchange is the description of the coupling, or influence of one moment over another, as a result of their wavefunctions overlapping, which can lead to electrons aligning parallel (ferromagnets) or antiparallel (antiferromagnets and ferrimagnets) to one another, with the alignment depending on the distance between the two unpaired electrons as well as the relative symmetry of the orbitals involved.

1.2.1.1 Direct Exchange

Direct exchange describes the coupling between two moments that lie close enough together to have their wavefunctions overlap directly. If the unpaired electrons on separate species are in close proximity and their respective orbitals overlap with one another, the electrons will be located between the atoms and align antiparallel to each other in order to obey the Pauli Exclusion Principle. In cases where the atoms are further apart, the electrons will minimize electron-electron repulsion and distance themselves from each other, which cause the electrons to align parallel to each other, giving rise to ferromagnetic coupling.

1.2.1.2 Superexchange

Superexchange occurs when two moments are too far apart to interact directly, and must couple through species that do not contain unpaired electrons such as O^{2-} or CN^{-}. One well known example of superexchange occurs in the Prussian Blue magnet with the formula $Fe^{3+}{}_4[(Fe^{2+}(CN)_6)^{-4}]_3$ (9) (10). Prussian Blue and its analogues contain (among other species)

metal ions with unpaired electrons bridged by cyanide (CN^-) ligands. If the metal d orbitals containing unpaired electrons are of the same symmetry, they can overlap with the antibonding orbital of the cyanide and the unpaired electrons of the metals will couple antiferromagnetically through the newly-formed set of molecular orbitals.

1.2.1.3 Indirect and Itinerant Exchange

In addition to direct exchange and superexchange there are two other modes by which electrons can couple, known as indirect exchange and itinerant exchange. Indirect exchange arises from the coupling of localized moments through conduction electrons (electrons delocalized on the surface of a metal as described by the electron-sea model). Itinerant exchange involves the coupling between conduction electrons in metals (8). These exchange interactions are prevalent in atom-based magnets and do not usually occur within molecule-based magnets because the unpaired electrons in the metal and molecular orbitals are localized.

1.2.2 Ordered States

The electronic "picture" of a paramagnet is generally described as one with unpaired electrons randomly oriented throughout the structure with little to no communication between spins. At specific temperatures (which will be explained below) in some materials, however, the influence of individual moments over one another begins to increase, which in turn can lead to ordered states. Scientists have discovered several types of magnetically ordered states exhibited by different solids, which arise due to neighboring electrons influencing one another in a manner where spins begin to align in certain, repeating arrangements.

1.2.2.1 Ferromagnetism and Antiferromagnetism

Ordered states in magnetic materials describe the way spins align with respect to each other throughout the solid. These ordered states include ferromagnetism, where the electron spins

align parallel to each other and generate a net magnetic moment, and antiferromagnetism, where the electron spins align antiparallel to each other which leads to cancellation of spins and does not result in a net magnetic moment. There are special cases of antiferromagnetism, however, that lead to a net magnetization, namely helimagnetism, canted antiferromagnetism, and ferrimagnetism.

1.2.2.2 Helimagnetism

Helimagnetism results from structures that have a base plane of moments aligned in the same direction and successive planes with moments inclined at some angle between 0 and 180 with respect to the moments on the plane beneath it (spins aligned at 0 and 180 degrees can be thought of as being either ferromagnetically or antiferromagnetically coupled to the spin of the base plane). This staggered orientation of spins leads to a helical structure, resulting in a net magnetic moment perpendicular to the planes. The solid $Eu(As_{0.20}P_{0.80})_3$ is an example of a helimagnet, with a T_N of 10.3 K (11).

1.2.2.3 Canted Antiferromagnetism and Ferrimagnetism

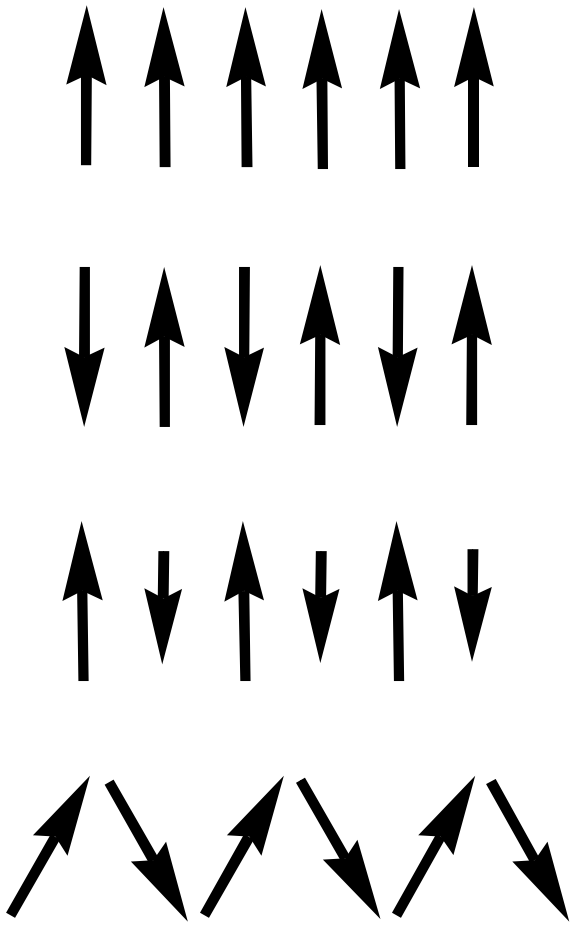

Figure 2. Depiction of magnetic moments aligned in various ordered states from top to bottom: Ferromagnetism, Antiferromagnetism, Ferrimagnetism, and Canted Antiferromagnetism.

In the case of canted antiferromagnetism, the orientation of the spins resemble that of antiferromagnets, but the spin orientations are canted in a new direction due to the structure of the solid, resulting in a net magnetic moment along that new direction (Figure 2). An example of a canted antiferromagnet is $CoCO_3$ (high-spin), which has a calcite crystal structure (12). Ferrimagnetism exists in materials where spins on adjacent sites are opposite in direction, but are unequal in magnitude, resulting in a non-zero magnetic moment. One example of this phenomenon is in the naturally occurring mineral magnetite (Fe_3O_4), which contains alternating Fe^{2+} (4 unpaired electrons) and Fe^{3+} (5 unpaired electrons) ions in the crystal lattice separated by oxygen anions.

1.2.3 Critical Temperature

1.2.3.1 Phenomenon

One of the most important concepts in magnetism is the critical temperature, which indicates the transition from an ordered magnetic state to a disordered state as a result of increased thermal energy overcoming the exchange energy associated with individual moments. Increased dimensionality in the ordered state is a result of larger exchange interaction strengths

and increases the amount of thermal energy required for a transition to a disordered state (13). For example, a solid with two-dimensional order will require more energy for randomization of its moments than a solid with one-dimensional chains, and three-dimensional order will require even more energy. Ordered states with higher dimensionality contain moments that have more nearest neighbors, increasing the number of exchange interactions surrounding each moment that must be overcome.

1.2.3.2 Curie and Néel Temperatures

For ferromagnets and ferrimagnets, the critical temperature is known as the Curie temperature T_c and for antiferromagnets, the critical temperature is referred to as the Néel temperature T_N. At temperatures below the T_c, the moments are aligned parallel or antiparallel to each other in ferromagnets and ferrimagnets, respectively, and a net magnetization is observed. The T_c of a magnet is an important factor when deciding whether that particular material should be used in an application, since it defines the conditions under which the magnet can function.

1.3 Magnetic Measurements

1.3.1 SQUID Magnetometer

SQUID (Superconducting Quantum Interference Device) magnetometry enables scientists to perform highly sensitive magnetic experiments (with sensitivity down to 10^{-8} emu at 2,500 Oe) on solid samples that measure magnetization as a function of both temperature and applied magnetic field. The working part of a SQUID consists of a superconducting ring with a small layer, known as a Josephson junction. Upon the ring becoming superconducting, the flux passing through the ring becomes quantized. The Josephson junction allows the flux in the ring to change by discrete amounts, which can be measured (14). Since the temperature of SQUID magnetometers is controlled with liquid helium, temperature dependent measurements can be

performed as low as 1.8 K which is necessary since many solids have drastically different magnetic properties at lower temperatures (dysprosium, for example, transitions from a paramagnetic state to a ferromagnetic state at 88 K).

Figure 3. Superconducting Quantum Interference Device (SQUID) magnetometer.

1.3.2 Magnetization vs. Temperature Measurements

The SQUID's ability to perform temperature dependent magnetic measurements provides a method for determining the T_c or T_N of materials. Plots displaying the magnetization of a magnet as a function of temperature are typically generated for field-cooled samples, or samples that are cooled from room temperature to low temperature (typically 5 K or below) under the influence of an applied field. After reaching the desired low temperature, the magnetic sample is then warmed in an applied field, and the magnetization is measured in chosen intervals (typically 10 K) up to the desired ending temperature. The shape of an M vs. T plot for ordered solids

resembles a plateau, with a characteristic steep drop in magnetization approaching zero (the magnetization does not go to zero, as some electron spins are still aligned with the field as the sample turns paramagnetic). The T_c, for the purpose of this study, is understood to be the extrapolation of the steepest part of the curve to zero magnetization (see Figure 4).

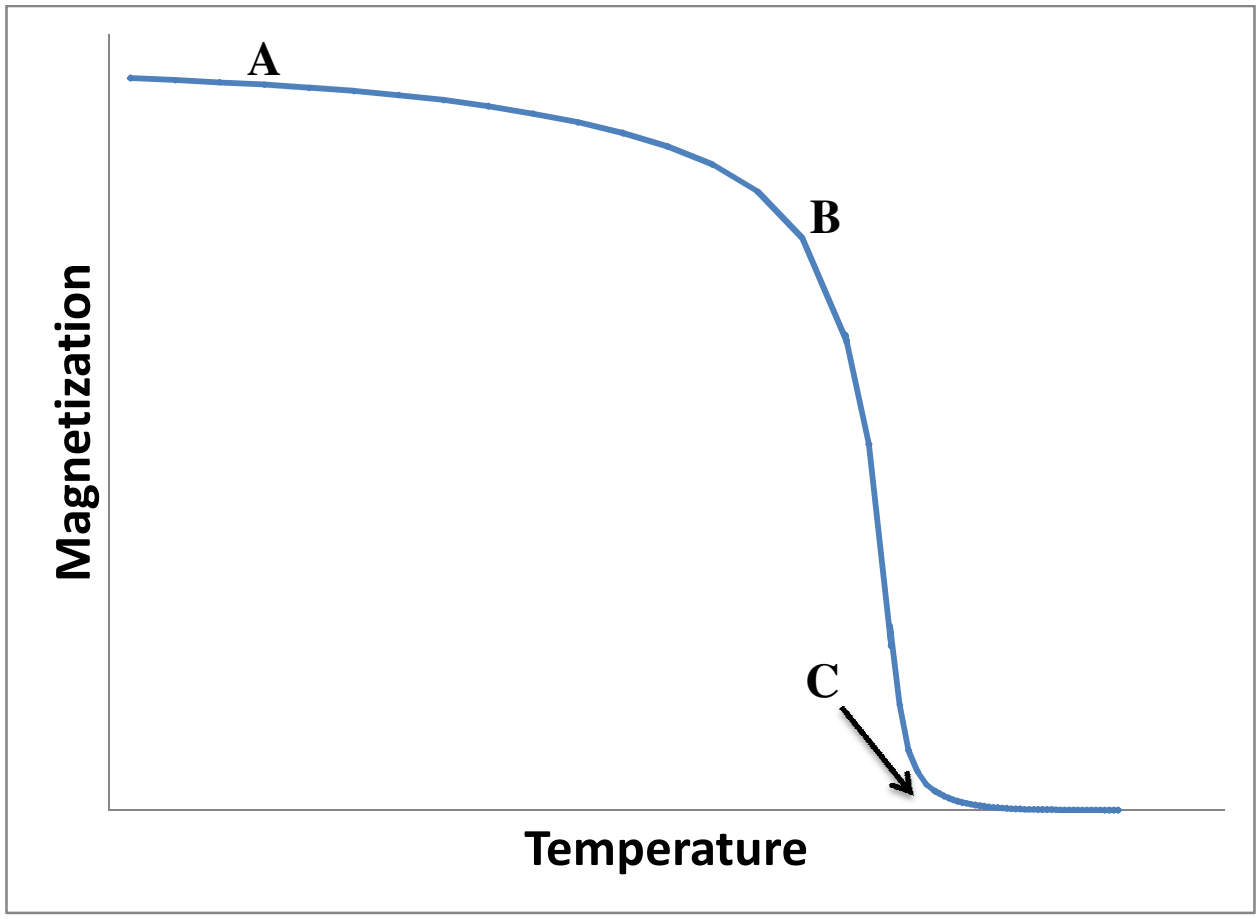

Figure 4. Three phases of a magnetization versus temperature plot based on the ferrimagnet V[4-MePTCE]2. A) ordered state, B) transition from an ordered state to a disordered state, and C) T_c of the sample, represented by the extrapolation of the steepest part of the curve to the x-axis.

1.3.3 Magnetization vs. Applied Field Measurements

Measuring the magnetization of a sample as a function of applied field can also yield useful information such as the coercivity and remanence of a magnet (explained below). With temperature held constant, the SQUID can measure the magnetization of a sample at varying applied fields by starting at zero field, increasing until the sample reaches saturation (or any

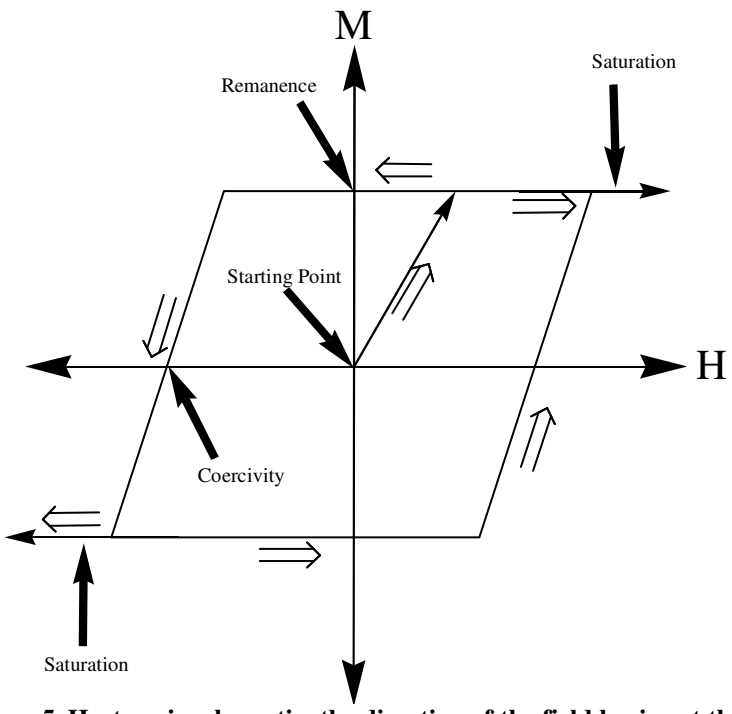

Figure 5. Hysteresis schematic; the direction of the field begins at the origin and follows the hollow arrows.

desired applied field), then decreasing the field to and past zero until it saturates the sample in the opposite direction, followed by returning the field to zero. These plots show whether the sample exhibits hysteresis, which is the irreversible magnetization (deviation of magnetization values from those resulting from the initial saturations) of a sample under the influence of changing applied fields. Hysteresis measurements can describe how easily a material is demagnetized (the reducing of magnetization in a sample to zero), which is another factor that determines whether a material is suitable for a particular application. The first property that can be observed is how wide or narrow the loop is along the applied field axis (x-axis), which is indicative of the coercivity, or the amount of applied magnetic field needed to reduce the magnetization of the magnet to zero after saturation.

1.3.3.1 Coercivity

Coercivity within a magnetic sample arises from two sources; crystal structure and orbital angular momentum. In magnetic solids, magnetic moments tend to align with certain crystallographic axes in order to achieve lower energies. When a magnetic field is applied, the moments will re-align themselves along with the axis closest to the field direction. This mechanism leads to lower energy, which results in coercivity. Coercivity is also dependent on

the anisotropy generated by the contributions from the orbital angular momentum within the electronic structure of the material, with larger orbital contributions resulting in larger anisotropies, thus giving larger coercivities. Anisotropy may arise from degenerate atomic orbitals capable of transforming into one another with a different spin state through some symmetry operation (for instance, the d_{xy} orbital can be rotated 90° to "transform" into the d_{yz} orbital, but this is not possible for the d_z^2 orbital since it does not resemble any of the other d orbitals). If all of the degenerate orbitals have the same occupancy (i.e., the d_{xy}, d_{xz}, and d_{yz} orbitals all contain unpaired m_s =1/2 spins), however, no anisotropy arises, and the orbital angular momentum is said to be quenched. Evidence of this theory is present in the literature, where magnetic systems that should not exhibit an orbital angular momentum show very small coercivities, and vice versa.

An example of this is present in Miller's work with the $M[TCNE]_2$ system, where if the metal is V^{2+} (d^3), the coercivity is small; however, if Fe^{2+} (d^6, high spin) is utilized, a substantial coercivity is observed (15). The coercivity of a magnet describes how hard or soft that magnet is, with high coercivities (> 20 Oe) corresponding to hard magnets and low coercivities (< 20 Oe) corresponding to soft magnets.

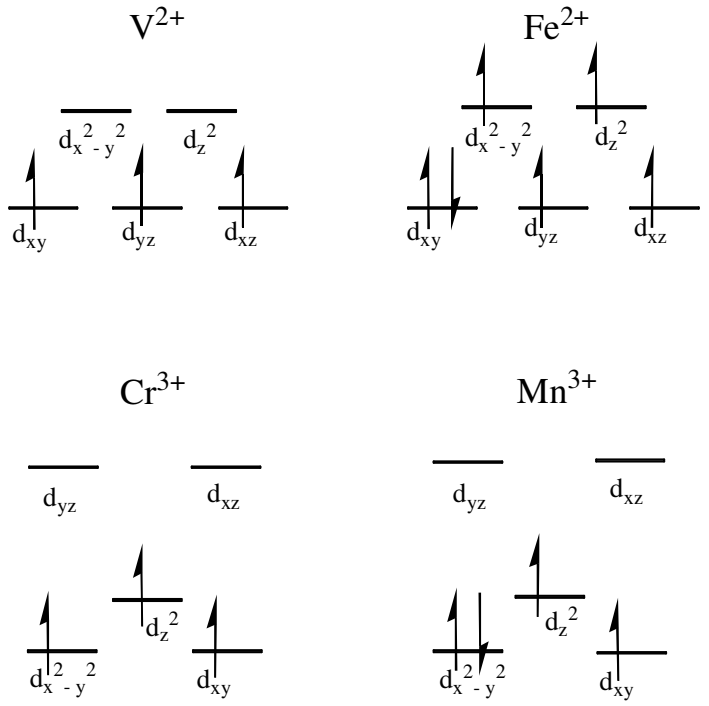

Figure 6. d-Orbital splittings for V^{2+} and Fe^{2+} In the M[TCNE] system and Cr^{2+} and Mn^{2+} in the [decamethylmetallocene]$^{+}$ [TCNE]$^{-}$ system. The electron configurations suggest that V and Cr should exhibit small coercivities, while Fe and Mn should exhibit large coercivities, which has been confirmed experimentally.

1.3.3.2 Remanence

Another piece of information obtained from a hysteresis loop is the remanence, which is described as the magnetization remaining in the material after the applied field has reached saturation and returned to zero. Remanence values correspond to the point of an M vs H curve where the hysteresis loop crosses the y-axis, and are indicative of the amount of magnetization a material can hold in the absence of any externally applied field.

2. Molecular Magnetism

2.1 Introduction, Definition

The term "molecule-based magnet" has been described in various ways, but the most widely accepted definition is a magnet in which spins contributing to the overall spin state are

localized on or communicate through molecular orbitals on molecules. With the discovery of the linear chain charge-transfer (CT) salt [$FeCp^*_2$][TCNE] ($FeCp_2^*$ = decamethylferrocene, TCNE = tetracyanoethylene) (16), which shows ferromagnetic behavior at low temperature, the field of molecule-based magnets has become one of importance and experienced quite a number of advances. Two other major discoveries in the field that have also had an impact are the discoveries of Prussian Blue analogues in the 1950's (9) (10) (Prussian Blue itself was discovered in 1704 in Germany), and the three-dimensional $V[TCNE]_2 \cdot yCH_2Cl_2$ system (17). The $V[TCNE]_2$ magnet is a ferrimagnet, while the Prussian Blue analogues can form ferrimagnets, ferromagnets or antiferromagnets. These two magnet systems are remarkable in that certain Prussian Blue analogues (18) and $V[TCNE]_2$ (17) are magnetically ordered above room temperature. Research of these two systems has yielded related groups of magnetic materials (to be discussed later) and a better understanding of how they function. The concept of being able to fabricate air-stable, room temperature magnets that are organic-based is very enticing due to the numerous advantages these magnets give (6) such as tunability and more convenient synthetic routes (i.e, synthesizing an atom-based magnet such as $SmCo_5$ requires heating to temperatures above 1000 °C (19), while $V[TCNE]_2$ can be synthesized at room temperature) than most atom based magnets. Apart from being more lightweight and processable than their fully metallic counterparts, organic-based magnets also possess a greater ability to be tuned electronically (through the use of various organic molecules), which has been shown to give different ordering temperatures and overall different magnetic properties.

2.2 $V[TCNE]_2$

2.2.1 Background

Following the discovery of the [FeCp*$_2$][TCNE] CT salt, there was the need to explore different donors and acceptors to gain further insight about the way the system worked. Manriquez and coworkers used V(C_6H_6)$_2$ with TCNE (to continue testing first row transition metals with unpaired electrons) but did not form the characteristic one-dimensional stacks observed when using other sandwich complexes. The vanadium was oxidized ($V^0 \rightarrow V^{2+}$), donating an electron to two TCNE's to form the radical anions. The TCNE radical anions coordinated to the vanadium ions, giving rise to a three-dimensional, ferrimagnetic solid that was magnetically ordered above room temperature (17). Each V^{2+} is S=3/2, and every $TCNE^{\cdot-}$ is S=1/2, so with a 2:1 ratio of acceptor to vanadium ions (determined by elemental analysis), the overall spin on the formula unit would be 1/2 through direct exchange, which explains the net magnetization of the air-sensitive amorphous solid, which can order up to 396 K (20). The bonding of TCNE to vanadium is further evidenced by the absence of benzene in the infrared spectrum of the product (21). The V[TCNE]$_2$ magnet has spawned a great deal of interest in molecule based magnets, with research efforts in several areas, including structure determination, solvent studies, and metal replacement studies.

$$2\ TCNE + V(C_6H_6)_2 \xrightarrow[N_2\ atmosphere]{CH_2Cl_2,} V^{II}[TCNE]_2 \cdot y\ CH_2Cl_2 + 2\ C_6H_6$$

Figure 7. Reaction of TCNE and V(C_6H_6).

2.2.2 Structural Studies

The structure of the magnet continues to elude researchers, as the solid formed is highly disordered, with no apparent pattern, indicating the mechanism involved with the reaction may be dominated by kinetics. A recent study has yielded powder diffraction pattern of Fe[TCNE]

that shows Fe^{2+} ions coordinated by six N atoms in an octahedral fashion (22). It has been confirmed through XANES (x-ray absorption near-edge spectroscopy) and EXAFS (extended x-ray absorption fine structure) studies that the vanadium is indeed surrounded by six nitrogens, which supports the theory on the geometry of the system (23). The oxidation state of the vanadium was also confirmed to be +2, which supports the theory that each vanadium was S = 3/2.

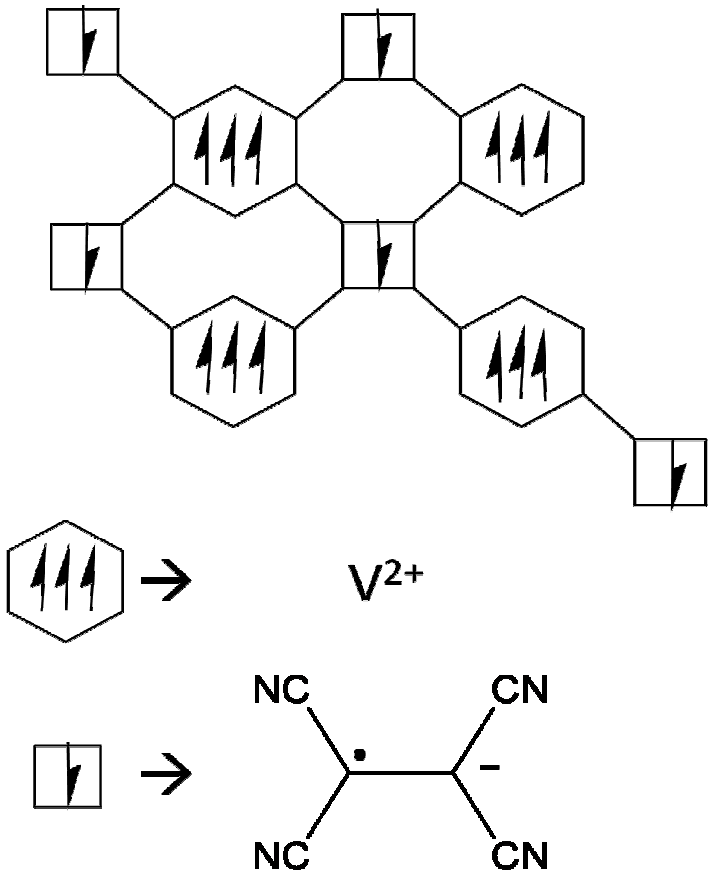

Figure 8. 2-D representation of the V[TCNE]$_x$ magnetic polymer network.

2.2.3 Solvent Studies

Many solvents have been used in the V[TCNE]$_2$ system, and it was found that when the reaction described above was performed in different solvents, a range of ordering temperatures were observed (20). Generally, non-coordinating solvents, such as dichloromethane (CH_2Cl_2) or

toluene (PhMe), tend to give higher ordering temperatures than coordinating solvents such as acetonitrile (CH_3CN). The highest T_c reported for $V[TCNE]_2$ was 396 K, when using α,α,α-trifluorotoluene ($PhCF_3$) as the solvent, which is possibly a result of its high dielectric constant (20). Coordinating solvents like acetonitrile can occupy sites on the V^{2+} ions, which can effectively decrease the number of $V^{2+}/TCNE^{\cdot-}$ connections, thus reducing T_c for the material (more V^{2+}/acceptor connections per vanadium lead to higher ordering temperatures). Shown below are the ordering temperatures for $V[TCNE]_2$ magnets of varying solvents and vanadium sources.

Table 1. T_cs of the $V[TCNE]_x$ magnet using various solvents.

Vanadium Source	Solvent	T_c (K)	Reference
$V(C_6H_6)_2$	CH_2Cl_2	350	(17)
$V(C_6H_6)_2$	THF	215	(24)
$V(C_6H_6)_2$	MeCN	138	(25)
$V(CO)_6$	CVD (no solvent)	370	(26)
$V(CO)_6$	CH_2Cl_2	387	(20)
$V(CO)_6$	PhMe	390	(20)
$V(CO)_6$	$PhCF_3$	396	(20)
$V(CO)_6$	Hexane	388	(20)

A separate study investigating a new acceptor to substitute for TCNE yielded results that could provide more information concerning solvent effects in the system. When dicyanoperfluorostilbene (DCPFS) was used as the acceptor in the vanadium reaction (the product of which exhibited magnetic order), it was found that using coordinating solvents actually increased T_c relative to using non-coordinating solvents (26). This result could be due

to coordinating solvents occupying any open sites on the V^{2+} ions not coordinated by the dicyano acceptors, which only have two possible coordinating nitriles as opposed to the four that TCNE possesses. Vacant sites on the V^{2+} ions might react with non-coordinating solvents in a way that is detrimental to the T_c (i.e., oxidative addition with dichloromethane). The dicyano acceptor, as well as other acceptors used to replace TCNE, will be discussed in detail in a later section.

2.2.4 Metal Replacement Studies

Experiments have also been conducted to test other divalent metals in place of vanadium, in efforts to make the product more air-stable. These magnets owe their air sensitivity largely to the oxophilicity of vanadium in its 2+ state. Other metals used in the synthesis include divalent ions of Mn, Fe, Co, and Ni (all using MI_2 as the precursor), none of which possessed an ordering temperature above 130 K (Mn=107 K, Fe=121 K, Co=44 K, Ni=44 K) (15). In an attempt to utilize another d^3 metal, niobium was also reacted with TCNE, the product of which only exhibited antiferromagnetic behavior (21). While these metal replacement studies provided new magnets, there is no correlation between the T_c values and the number of spins on each metal cation or the *J* values calculated for each ion (15).

2.2.5 TCNE Dimers

One factor that researchers have hypothesized as a problem for this system is the formation of π-stacked $(TCNE)_2^{2-}$ dimers, which are diamagnetic and cannot contribute to the overall magnetic order of the solid (27). One way to avoid this potential problem was to synthesize TCNE analogues with CN groups replaced by a bulkier group, such as a phenyl ring, which could possibly block the π-stacking interactions.

2.2.6 Alternatives to TCNE

One of the first of such analogues was dicyano(perfluoro)stilbene (DCPFS). When DCPFS was reacted with $V(CO)_6$, the product exhibited ferrimagnetic ordering below 205 K (26), suggesting that four nitrile bridging sites were not required to achieve magnetic ordering. Tetracyanoquinodimethane (TCNQ), provided an electron-poor acceptor with the option of substitution at the 2 and 5 positions of the ring, with strong electron-donating groups giving the highest T_c (28). Substituted aryl rings were also studied. Tetracyanobenzene (TCNB) and tetracyanopyrazine (TCNP) which exhibited T_c values of 323 K (29) and 200 K (30), respectively, while hexacyanodivinylbenzene only ordered below 120 K (31). While the acceptors mentioned above demonstrate the variety of bridging one-electron acceptors that can be utilized to synthesize magnetic polymers, until this point there was no acceptor suitable for a library approach that closely resembled TCNE in its magnetic environment with V^{2+}.

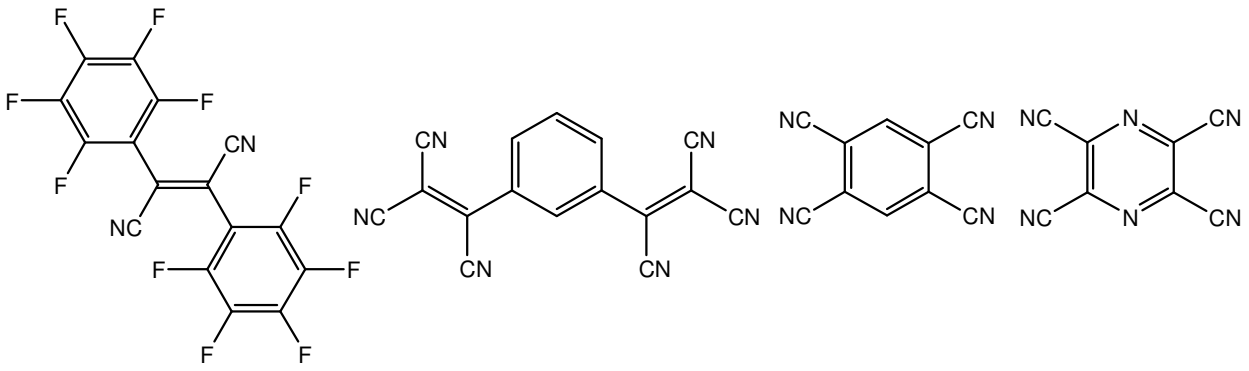

Figure 9. Various electron-poor acceptors used in the V[acceptor]$_x$ synthesis from left to right including T_cs: dicyanoperfluorostilbene (205 K), i-hexacyanodivinylbenzene (120 K), tetracyanobenzene (325 K), and tetracyanopyrazine (200 K).

2.3 PTCE

2.3.1 Introduction

Another substitute for TCNE involved replacing only one nitrile with a phenyl ring, to determine if fewer nitrile groups corresponded to increases in T_c. Phenyltricyanoethylene (PTCE) and its substituted analogues are structurally more similar to TCNE than the previously mentioned acceptors. The PTCE molecule and its substituted analogues can be easily synthesized

from the corresponding benzaldehyde and malononitrile (32). The first PTCE to be used in the magnet synthesis was (pentafluorophenyl)tricyanoethylene (F_5PTCE) (31), which reacts with $V(CO)_6$ to give a product that is magnetically ordered above room temperature, around 307 K (33). This made F_5PTCE the only acceptor other than TCNE in this system at the time with a T_c above room temperature. The magnet based on the unsubstituted PTCE (H_5PTCE) magnetically orders below 215 K (33), a significant decrease from TCNE. This observation is reasonable and somewhat expected, considering that there is now one less CN group per acceptor to coordinate to the vanadiums, which could possibly lead to fewer exchange pathways. The π* orbital of PTCE has a higher orbital energy relative to that of TCNE, which could also factor into the decrease of T_c (as the energy gap between the π* orbital of the acceptor and the d orbitals of the metal increases, the exchange energy should decrease).

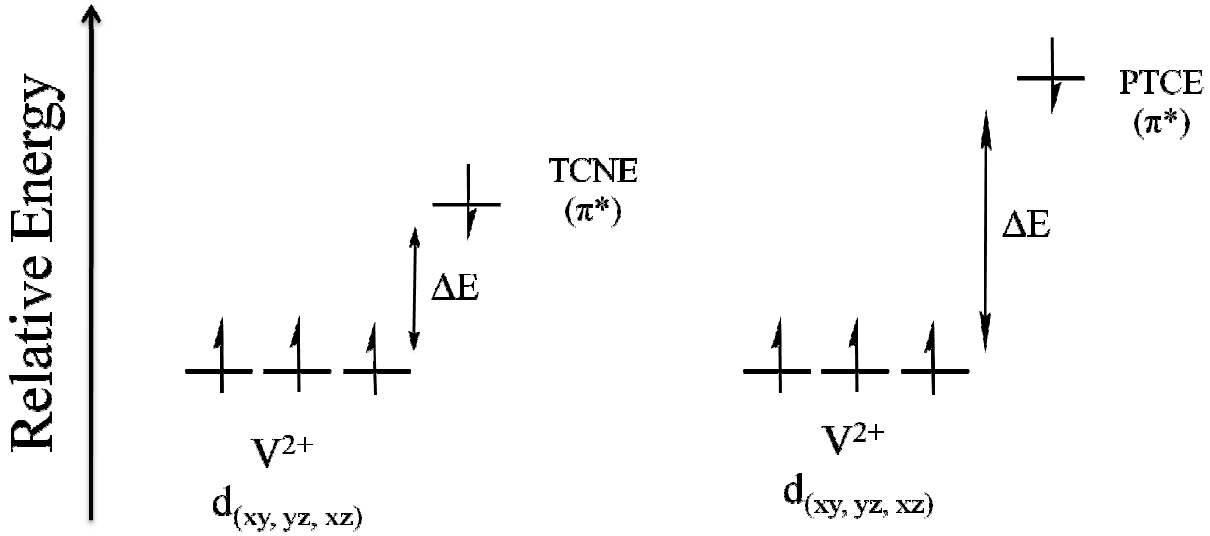

Figure 10. Relative π* energies of TCNE and PTCE with respect to the V^{2+} ion. Higher ΔE values correspond to lower exchange energies.

2.3.2 H_5PTCE and F_5PTCE

After realizing that the new acceptor still formed a magnetic solid, albeit one that ordered at a lower temperature, the next step was to substitute the phenyl ring with functional groups

(33). The H_5PTCE and F_5PTCE acceptors were thought to serve as the lower and upper limits, respectively, for any fluoro-substituted acceptors in terms of ordering temperature, because it was assumed that adding any fluorines would lower the energy of the π* orbital. Initial research focused on finding substituents that would help lower the energy of the lowest unoccupied molecular orbital (LUMO), with the idea that if the acceptor LUMO and the d orbitals on the metal were closer in energy, T_c would increase (the exchange interaction increases if the unpaired electrons are closer in energy). With that idea, the Yee group began to synthesize acceptors with fluorinated phenyl rings attached to the tricyanoethylene moiety, with the idea that fluorine, which is known to be electron withdrawing, would lower the electron density of the ring, thus lowering the energy of the LUMO.

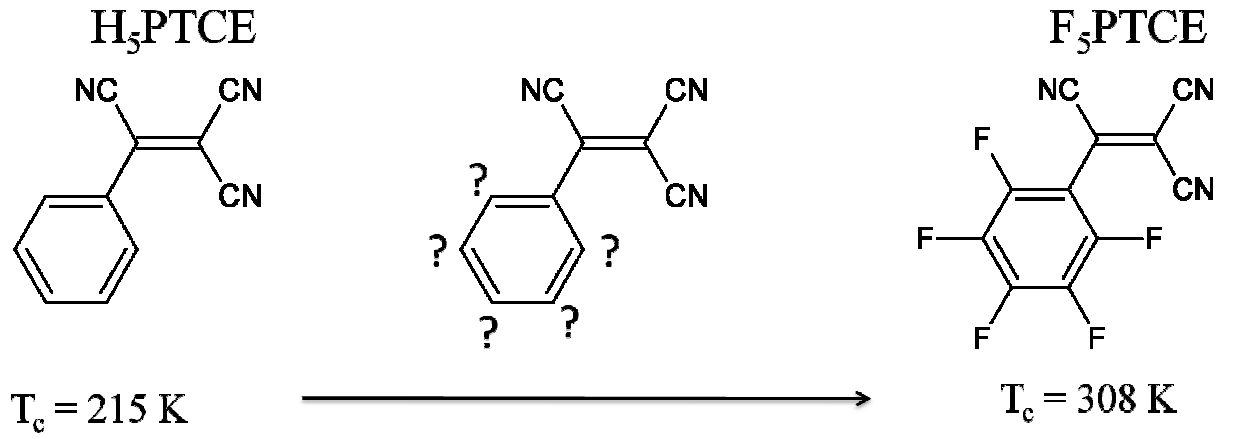

Figure 11. Ordering temperatures of H_5PTCE and F_5PTCE, previously thought of as the lower and upper limits, respectively, for F_xPTCE-based magnets.

2.3.2 F_xPTCE

Magnets of various acceptors were synthesized, using phenyl rings that were mono, di, and tri-substituted with fluorines. Most of the T_c's fell between the H_5PTCE and F_5PTCE T_c's, showing that substituting the 3 and 5 positions gave better ordering temperatures and substituting the 2 and 6 positions gave the best ordering temperatures (34). The 4-fluoro acceptor-based magnet ordered at 159 K (34), well below the H_5PTCE T_c, and the 2,3,5,6-tetrafluoro acceptor-

based magnet (unpublished work, M. Harvey) ordered above the F_5PTCE, indicating that substituting in the 4 position of the phenyl ring is detrimental to the T_c of the magnet. This was also evident when comparing the T_c's of the 2-FPTCE (259 K) and 2,4-diFPTCE (244 K) (34).

2.3.4 $(CF_3)_x$PTCE (Unpublished work, A. Wells and A. Amshumali)

Fluorines (and the halogens, for that matter) are thought to be electron withdrawing by inductance and electron donating by resonance, so in order to find whether inductance or resonance had the greater influence on the ordering temperature, a new family of acceptors with trifluoromethyl (CF_3) groups substituted around the ring was introduced. CF_3 is considered to be strongly electron withdrawing, and would provide insight to the effect of electron withdrawing groups on the ring. CF_3 groups substituted in the 2 and 3 positions on the ring showed the same general pattern as any of the other substituents (2 orders higher than 3), but when in the 4 position, CF_3 elevates the T_c (230 K) of the polymer relative to the H_5PTCE molecule. This observation has led to the hypothesis that electron donation of any magnitude on the 4 position is detrimental to the ordering temperature.

Table 2. T_c values of V[X-PTCE]$_x$ magnets (X = F, Cl, Br). * This work.

Position	-F	-Cl	-Br	-CF_3	-CH_3*
2-	255 K	270 K	265 K	259 K	244 K
3-	238 K	230 K	-	220 K	200 K
4-	159 K	139 K	118 K	235 K	182 K

2.3.5 EDG$_x$PTCE?

With all of the research that has been done thus far, a systematic study involving substituents that are strictly donating in nature has not surfaced. The hypothesis, based on experimental evidence, is that donating groups should lower T_c values when PTCE reacts with

$V(CO)_6$. The gap in energy between the electrons involved will be larger with the PTCE molecules containing donating groups than those containing withdrawing groups. In addition to the electronic effects of different PTCE analogues, there is also a question concerning steric hindrance; the dihedral angle (specifically between the olefin and phenyl ring) of the PTCE molecule may be significantly influenced by the groups substituted on the ring, especially those in the ortho positions.

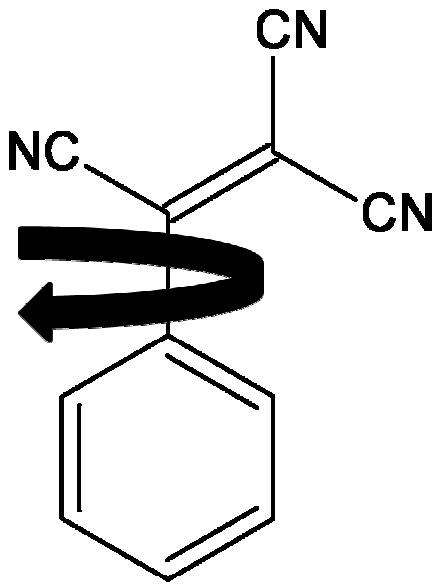

Figure 12. Rotation within the PTCE molecule between the phenyl ring and olefin moeity.

In order to address these concerns, PTCE molecules containing methyl ($-CH_3$) groups will be the focus of a study that involves analyzing the acceptors and the magnets that result from their reactions with vanadium. The methyl group is a good choice for furthering the work done in this field for several reasons. Methyl groups are known to be slightly donating with no appreciable withdrawing capability, which is useful for confirming that donating groups are indeed detrimental to ordering temperature. Also methyl groups are similar in size to trifluoromethyl groups, so any deviations in steric hindrance going from trifluoromethyl to methyl will be minimal.

3. Results and Discussion

3.1 Acceptors

The PTCE acceptors reported thus far have contained groups that are either strictly withdrawing or capable of withdrawing and donating, but there has not been systematic study of substituents that are strictly donating. Methyl-containing analogues of PTCE may be obtained in a 3-step synthetic route that typically results in yields of 10-15%, based on the benzaldehyde analogue used for each acceptor. A reaction schematic is shown below that depicts the synthesis of electron-poor PTCE molecules from derivatives of benzaldehyde.

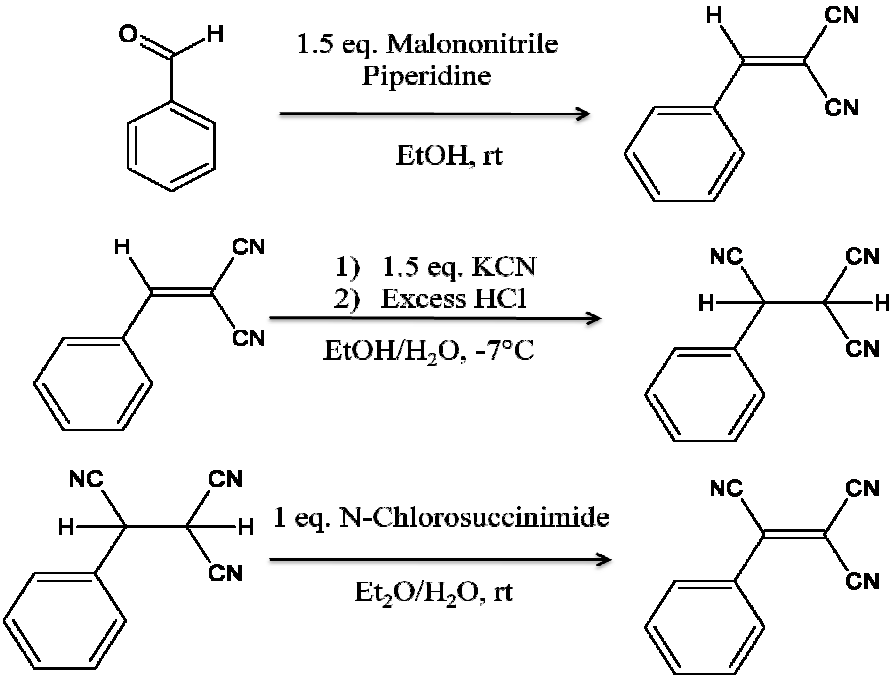

Figure 13. Reaction scheme for synthesizing PTCE starting from benzaldehyde.

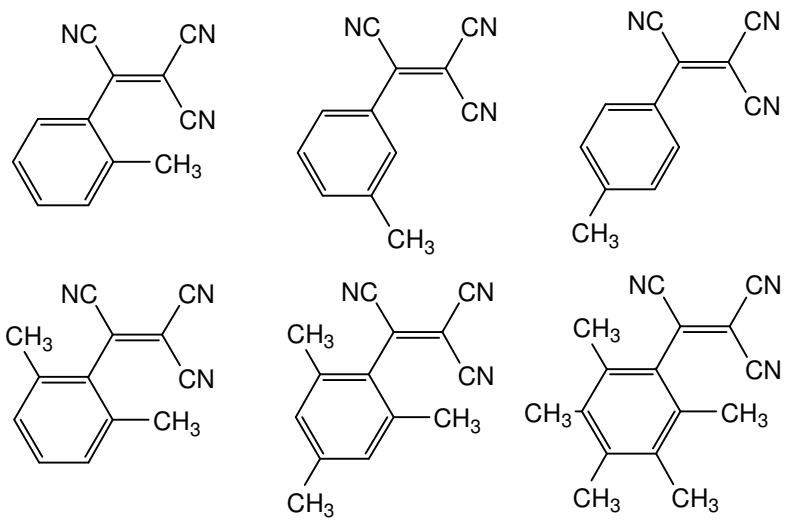

Figure 14. Methyl-substituted phenyltricyanoethylenes.

3.1.1 Electronic Effects

The selection of these methyl-containing PTCE molecules for use as acceptors in the magnet synthesis is the result of group discussions involving the electronic effects of the acceptor on the ordering temperature of the resulting magnet. When compared to the unsubstituted PTCE-based magnet, acceptors that contained electron withdrawing groups increased the ordering temperature (with the exceptions being the fluoro and chloro para-substituted PTCEs). Methyl groups are known to be inductively electron donating, and provide the opportunity to explore the effects of increasing the electron density of the phenyl ring on the T_c of the magnet.

One way to assess the electronic effects of methyl groups is to measure rates of electrophilic aromatic substitution. Electron donating groups are known to increase the rate of substitution around the ring, particularly in the positions ortho and para to them due to resonance. Hence, donating groups are said to be activating and are known as ortho/para directors. Electron withdrawing groups are known to decrease the rate of electrophilic

substitution on the ring, and the resonance forms indicate that substitution occurs primarily in the meta position. Because of this, withdrawing groups are said to be deactivating and are known as meta directors. This knowledge combined with experimental results regarding the relative acidities of benzoic acid and substituted benzoic acids may help explain T_c trends involving monosubstituted acceptors.

The pK_as of methyl-substituted benzoic acids relative to unsubstituted benzoic acid offer another systematic approach to comparing the effects of the methyl group in different positions of the ring. The carboxyl group (-COOH) becomes stabilized if there is more electron density in its pi system, decreasing acidity. Likewise, less electron density in the pi system destabilizes the carboxyl group and makes it more likely to release its proton. The benzoic acid derivatives m-toluic acid and p-toluic acid have pK_as of 4.27 and 4.37, respectively. These values are higher than the pK_a of benzoic acid (4.19) which indicate the methyl groups are increasing the electron density of the phenyl ring. The p-toluic acid is weaker than the m-toluic acid because donating groups affect positions ortho and para to them to a greater degree than positions meta to them. The o-toluic acid, however, has a pK_a slightly lower (3.91) than benzoic acid. This increase in acidity can be explained by the steric hindrance of the methyl in the 2 position decreasing the conjugation between the phenyl ring and carboxyl group, therefore decreasing electron donation. This concept of steric hindrance directly affecting extended pi systems will become important when discussing results of the magnetic experiments below, especially in the case of the 2-MePTCE acceptor and magnet.

3.1.2 Steric Interactions

In addition to the argument of the effects of electronics on the magnets' ordering temperatures, steric hindrance from substituents on the phenyl ring may also affect the magnetic

properties of the resulting magnets, particularly in the ortho positions of the phenyl ring. Within the PTCE molecule one can define a dihedral angle between the phenyl ring and the olefin moiety, and the size of the group on the ortho ring position(s) can have a pronounced affect on that angle. The significance of the dihedral angle in these molecules lies with conjugation; if the dihedral angle is 0°, the pi system of the phenyl ring is fully conjugated with the pi orbitals of the olefin. If the angle is 90°, the two sections of the molecule are orthogonal, or there is no conjugation between the two.

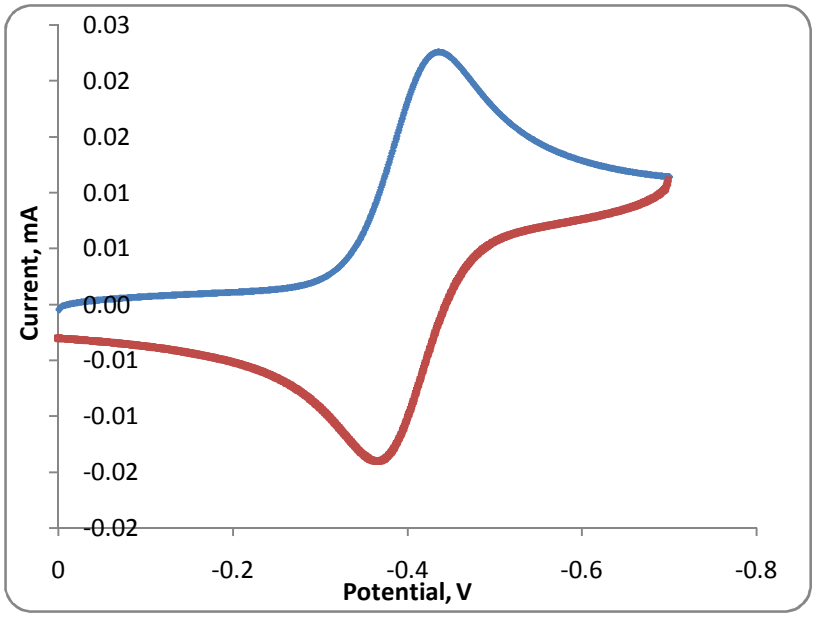

Figure 15. Cyclic voltammagram for 4-MePTCE. The top half of the data represents reduction and the bottom half represents oxidation.

The idea behind using larger groups in the ortho positions is that increasing the dihedral angle in PTCE through steric hindrance can destabilize the extended pi system of the molecule and possibly isolate the unpaired electron of the radical anion on the olefin portion. If the electron can be localized on the olefinic carbons, the exchange between it and neighboring unpaired electrons may be more effective, thus improving T_c.

3.2 Electrochemistry

3.2.1 Introduction/Results

One of the two fundamental properties of the acceptors used in this line of research is the ease with which the chosen acceptor can be reduced by one electron. This data can be obtained

using cyclic voltammetry (CV). Cyclic voltammetry experiments were performed on each of the acceptors chosen for this study in the hope that the reduction potentials and reversibilities obtained would help to explain why using certain acceptors results in higher ordering temperatures than others. The experimental details involved with the cyclic voltammetry are described in detail in the Experimental section, and the results are listed below.

Table 3. Electrochemical data of the Me_xPTCE acceptors.

Acceptor	E_{red} (V)	E_{ox} (V)	$E_{1/2}$ (V)
H_5PTCE	-0.437	-0.357	-0.397
2-MePTCE	-0.473	-0.407	-0.440
3-MePTCE	-0.431	-0.372	-0.402
4-MePTCE	-0.463	-0.402	-0.433
2,6-diMePTCE	-0.487	-0.425	-0.456
2,4,6-triMePTCE	-0.514	-0.453	-0.484
Me_5PTCE	-0.547	-0.482	-0.515

3.2.2 Discussion

All six acceptors exhibited one-electron reversibility with reduction potentials between -400 mV and -600 mV. This would suggest that these acceptors are more electron-rich than their

fluoro-containing counterparts which are easier to reduce (34). The reduction potentials would suggest that the PTCE molecule becomes more electron rich as more donating groups are added to the ring, with the exception of one instance. The 3-MePTCE molecule (-431 mV) shows a higher reduction potential (easier to reduce) than the original PTCE molecule (-437 mV), the 2-MePTCE (-470 mV), and the 4-MePTCE (-463 mV). This is also seen with the F_xPTCE acceptors, where the 3-FPTCE (-334 mV) is more easily reduced than the 2-FPTCE (-375 mV). A possible explanation for both of these results is that orbitals associated with the LUMO of these molecules do not reside on the meta carbons, making meta substituents irrelevant to the electronics of the system. If donation from the meta position is not a factor, a degree of steric hindrance from a methyl could increase the dihedral angle enough to help destabilize the pi system between the phenyl ring and olefin.

3.3 Density Functional Theory

3.3.1 Introduction

Using the B3LYP level of theory with the 6-31++G(d,p) basis set, the optimized geometries were calculated for each acceptor (neutral and radical anion). The goals of performing the DFT calculations were to determine the dihedral angles of the acceptors (both the neutral and radical anion forms) and to calculate the electron affinity of each acceptor. The Mulliken spin densities of the nitrile nitrogens of each acceptor (available in the raw output data files) were also recorded and analyzed. All calculations were performed in the gas phase.

3.3.2 Dihedral Angles

The first interest of these molecules involves the dihedral angle between the olefin moiety and the phenyl ring; if these molecules are assumed to be flat (dihedral angle = 0), the pi

system from the phenyl ring is fully conjugated with the pi orbitals of the olefin. As the dihedral angle increases due to steric hindrance, the conjugation decreases, effectively isolating an unpaired electron. According to the results of the DFT calculations, predictions about the non-planar structure of PTCE and its analogues were confirmed. Every neutral acceptor calculated gave a significant dihedral angle (greater than 20°), and every acceptor showed a decrease in the dihedral angle when the radical anion was calculated. The dihedral angles of each acceptor (neutral and radical anion) are listed in Table 5.

Figure 16. Two possible 0° geometries of 2-MePTCE, with the molecule on the right giving the higher energy.

In a separate set of calculations, the energies of the 3-MePTCE and 2,6-diMePTCE were calculated for dihedral angles between 0 and 180° in 10° increments. The purpose was to determine if there was a significant barrier to rotation of the phenyl ring. The 3-MePTCE and 2,6-diMePTCE were chosen because they represent the low-angle and high-angle groups, respectively. The 3-MePTCE molecule displayed a very low barrier to rotation (~9 kcal/mol), essentially allowing the phenyl ring to rotate freely. The issue that arises from this is if there is no barrier to rotation in the low-angle acceptors, then the dihedral angles that were calculated may not be relevant. More calculations will have to be performed to further support this hypothesis.

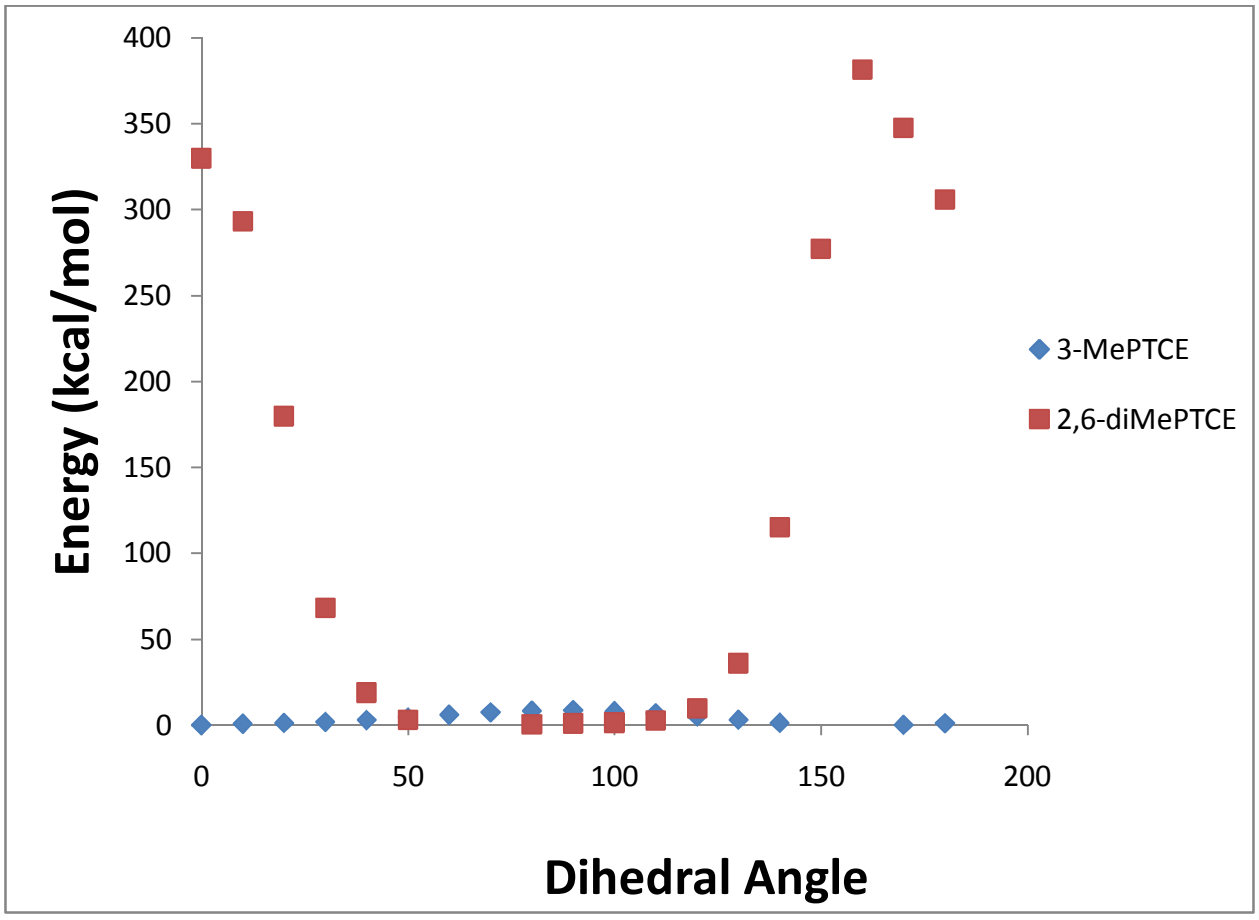

Figure 17. Plot of acceptor energies versus increasing dihedral angles. Calculations were performed by Gordon Yee as part of a private communication.

Table 4. Calculated values for the Me_xPTCE acceptors. All values were calculated using the B3LYP functional and the 6-31++G basis set.**

Acceptor	Dihedral Angle (neutral), °	Dihedral Angle (anionic), °	Electron Affinity, eV	Mulliken Spin Densities (Nitrogen atoms)	Mulliken Spin Densities (para carbon)
H_5PTCE	29.6	15.3	2.5598	0.417	0.138
2-MePTCE	52.6	39.2	2.4881	0.448	0.071
3-MePTCE	29.3	15.1	2.5168	0.416	0.138
4-MePTCE	25.9	15.3	2.4801	0.429	0.145
2,6-diMePTCE	75.0	63.4	2.4523	0.482	0.020
2,4,6-triMePTCE	70.4	63.7	2.4044	0.476	0.034
Me_5PTCE	78.8	67.6	2.3188	0.488	0.007

3.3.3 Electron Affinities

Electron affinities were calculated for each acceptor with the intention of correlating them not only to the ordering temperatures of the magnets, but also to the group of acceptors' reduction potentials. Reduction potentials and electron affinities are related phenomena (the addition of one electron to the LUMO, with the difference being that reduction potentials are measured in solution while electron affinities are calculated in the gas-phase) so there should be some correlation between the two. The calculated electron affinities followed a pattern similar to the electrochemistry results, with the Me_5PTCE and 2,4,6-triMePTCE displaying the lower electron affinities and the H_5PTCE and 3-MePTCE displaying the highest electron affinities. The electron affinities are listed in Table 5 and correlation with the other properties are discussed below.

3.3.4 Mulliken Spin Denisty

In addition to the dihedral angles and electron affinities, the Mulliken spin densities of certain atoms were analyzed. Of particular interest are the nitrogen atoms of the nitrile groups and the para carbons of the phenyl rings. The nitrogen atoms bind to the V^{2+} ions in the network, while the para carbons of the phenyl rings are also of interest due to the previous magnetic results of acceptors with para substitution. Acceptors with groups in the para position have (with the exception of the 4-CF_3PTCE acceptor) depressed T_c so a correlation between the para carbon and ordering temperature is also sought. The Mulliken spin densities are listed in Table 5, and their values are to be plotted and discussed below.

3.4 Infrared Spectroscopy

3.4.1 Results

The infrared spectra of V[acceptor]$_x$ magnets provide a useful method of confirming the reaction between vanadium and nitrile-bearing acceptors. When comparing the IR spectrum of the unreacted acceptor to the spectrum of the synthesized magnet, the key feature should be a shift of the C≡N stretch from higher wavenumbers in the acceptor to lower wavenumbers in the magnet. This shift is the result of one electron reduction combined with the nitrogen lone pair being used as a bonding pair, both of which make the C≡N bond weaker and stretching easier.

Table 5. Nitrile stretches of the acceptors and the resulting magnets.

Acceptor	Acceptor $\nu_{C\equiv N}$ (cm^{-1})	Magnet $\nu_{C\equiv N}$ (cm^{-1})
2-MePTCE	2240, 2247	2215, 2119
3-MePTCE	2234, 2196	2207, 2116
4-MePTCE	2235, 2198	2210, 2115
2,6-diMePTCE	2240, 2242	2202, 2116
2,4,6-triMePTCE	2238, 2245	2209, 2114
Me_5PTCE	2242, 2264	2219, 2113

3.4.2 Discussion

When comparing the IR spectra of the acceptors and magnets, a noticeable broadening of the nitrile stretches is observed, which is the result of several nitrile environments (28) within the polymer. In addition to the shift and broadening of the nitrile stretch, further evidence of the reaction is found when comparing the IR spectrum of the vanadium source (whether it be $V(CO)_6$ or $V(C_6H_6)_2$) to the spectrum of the magnet. The stretches that result from the CO molecules in the precursor are absent in the IR spectrum of the magnet due to the acceptors replacing the above mentioned ligand on the vanadium ions.

4. Magnetic Properties

4.1 Introduction/Summary of Synthesis

The magnetic studies described in this report are part of an ongoing effort to understand the factors that govern the properties of the M[acceptor]$_2$ magnet. While experiments involving magnetization vs. applied field are important for the characterization of the magnets, the magnetization vs. temperature measurements are necessary for establishing any trends involving T_c in the M[acceptor]$_2$ system. The following section is dedicated to the properties exhibited by the magnets that result from the reaction of $V(CO)_6$ and the methyl-containing PTCE molecules

described above. In addition to comparing the ordering temperatures presented here with previous data, attempts were made to correlate the ordering temperatures of the magnets with properties of the acceptors that were determined experimentally and theoretically.

When methyl groups are substituted on the phenyl ring of PTCE, the magnetic properties of the resulting magnets tend to follow the trend of their halogenated counterparts with comparable T_c values (Table 2). The trend seen in halogen-substituted PTCE molecules is that ortho substitution gives the highest T_c, with meta substitution giving lower ordering temperatures and para position giving the lowest T_cs. The T_c also increases when halogens are added symmetrically to the phenyl ring (groups in the 2 and 6 or 3 and 5 positions).

The results of magnetization vs. applied field experiments were similar to the results of all of the magnets in this system, as the magnets showed plots with no appreciable coercive fields. Comparing the similarities and differences between the group of magnets described here and the groups that were analyzed in the past (most importantly the fluorine and trifluoromethyl substituted PTCE molecules) provides information essential to establishing more trends within the $V[PTCE]_2$ system.

4.2 M vs. T Measurements

4.2.1 $V[2\text{-MePTCE}]_2 \cdot 0.32CH_2Cl_2$

The 2-MePTCE magnet displayed an ordering temperature (244 K) that was unexpected based on assumptions from previous experiments. The fact that the 2-MePTCE magnet orders higher than the unsubstituted PTCE magnet suggests that steric hindrance from the phenyl ring can and does play a significant role in determining T_c. The methyl group in the 2 position is thought to hinder the ring from aligning its pi system with the olefin, decreasing conjugation throughout the molecule. The T_c of the 2-Me magnet is most likely lower than the 2-FPTCE and

2-CF_3PTCE magnets because of the slightly donating nature of the methyl group. The π* orbital of PTCE is lower in energy with withdrawing groups attached (more favorable matchup with V^{2+} d orbitals) and higher in energy with donating groups attached (as evidenced by cyclic voltammetry, which is discussed below).

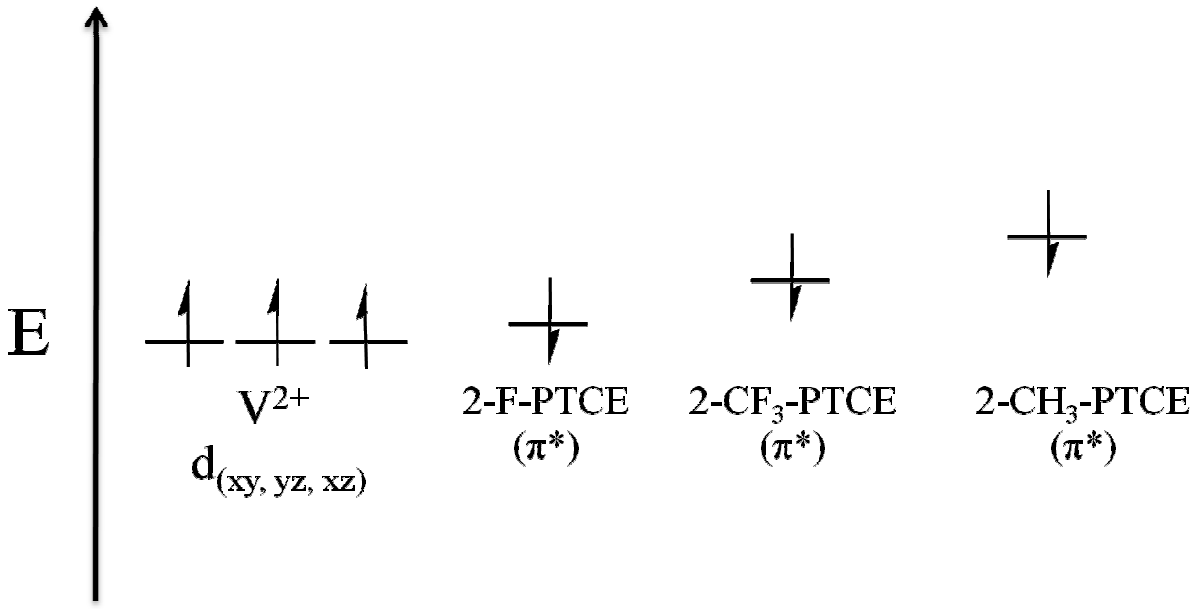

Figure 18. Relative π* orbital energies based on the reduction potentials of the 2-FPTCE (-0.375 V), 2-CF_3PTCE (-0.380 V) and 2-CH_3PTCE (-0.473 V) molecules.

4.2.2 $V[3\text{-MePTCE}]_{2.6}\cdot 0.08CH_2Cl_2$

Mono-substituting in the 3 position of the ring thus far has shown positive effects on T_c with respect to the unsubstituted acceptor (215 K), whether being significant in the case of the fluoro compounds(> 10 K difference), or not so significant with the CF_3 magnets(< 10 K difference). When substituted with a methyl group in the 3 position, however, T_c decreases to 200 K, which suggests that donating groups on the ring are detrimental to the ordering temperature of the magnet. This also suggests that steric hindrance from meta substitution on the dihedral angle between the phenyl ring and the olefin is negligible.

4.2.3 V[4-MePTCE]$_2$·0.55CH_2Cl_2

Another important observation is the T_c of the 4-methyl acceptor (180 K). Although the 4-Me magnet ordered lower than the H_5PTCE based magnet, it ordered higher than any other magnet with an acceptor that was monosubstituted in the 4 position, except for the 4-CF_3 acceptor (230 K). Alkyl groups, along with halogens, have the ability to donate electron density into the ring, whether through induction with the alkyls or pi donation as with the halogens. Electrons that are located in non-bonding orbitals are more easily delocalized than those located in bonding orbitals due to non-bonding orbitals being more diffuse, and is the most probable reason as to why the 4-Me acceptor orders higher than the 4-F, although lone-pair electrons on fluorine are not likely to be delocalized due to fluorine's high electronegativity. The trifluoromethyl group cannot donate in this fashion, which could explain why it is the only group currently known that increases T_c in the 4 position. This suggests that donating into the 4 position is not a favorable interaction, and should be avoided when synthesizing acceptors aimed at maximizing T_c.

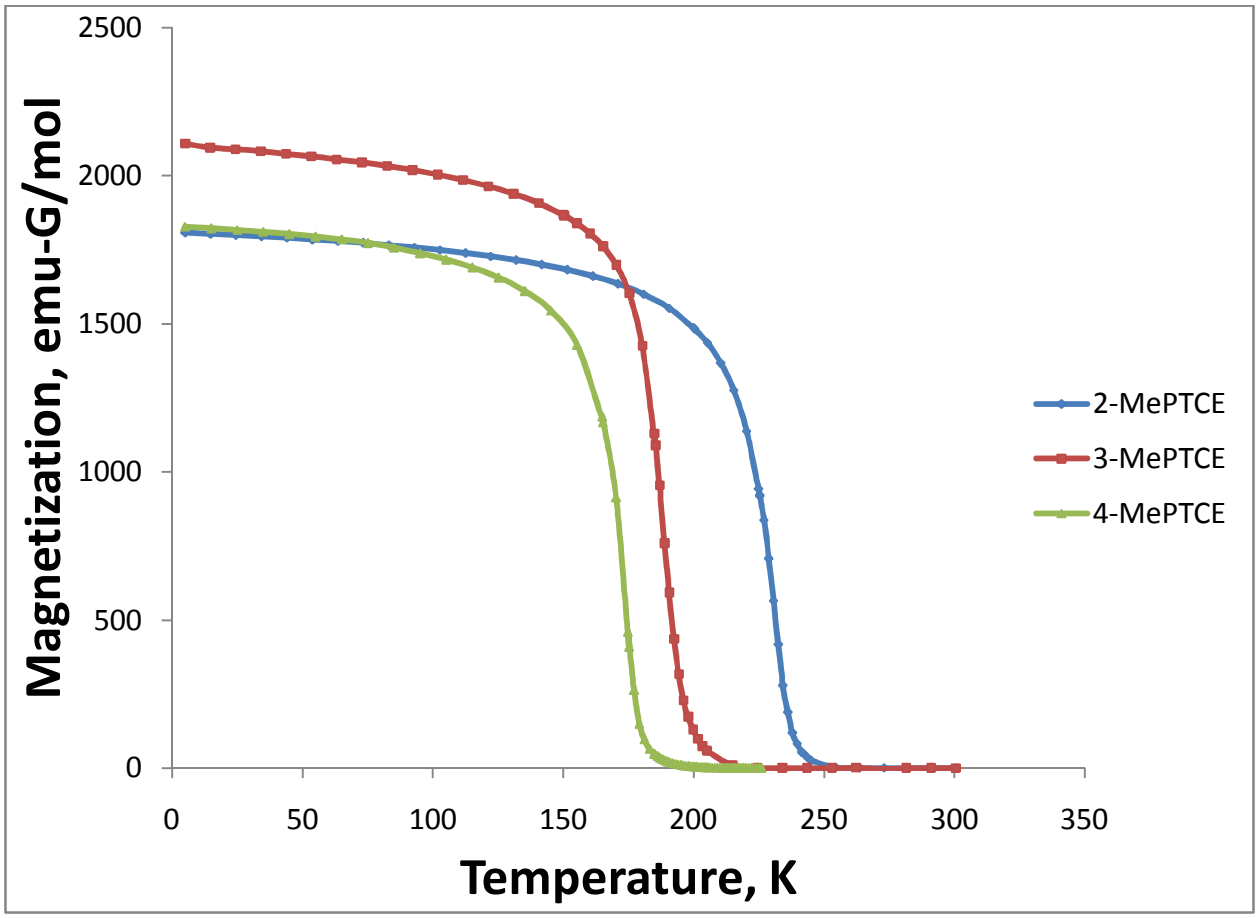

Figure 19. M vs T plots of 2, 3 and 4-MePTCE magnets.

4.2.4 V[2,6-diMePTCE]$_2$·0.26CH_2Cl_2

PTCE analogues with substituents in the 2 and 6 positions thus far have shown increases in T_c relative to 2-substituted PTCEs, but the data suggests that the donating ability of methyl groups (weak as it may be) negates this effect by raising the orbital energy. Substituting methyl groups in the 2 and 6 positions on the ring gave a slight decrease in T_c with respect to substitution in the 2 position alone (2-Me (245 K) → 2,6-di-Me (241 K)).

4.2.5 V[2,4,6-triMePTCE]$_2$·0.57CH_2Cl_2

To help support the theory that substitution in the 4 position decreases T_c, a PTCE acceptor with methyl groups in the 2, 4, and 6 positions was synthesized and used in the magnet

synthesis. As expected, the magnet based on the 2,4,6-triMe acceptor lowered T_c with respect to the 2,6-diMe magnet, resulting in an ordering temperature of 215 K.

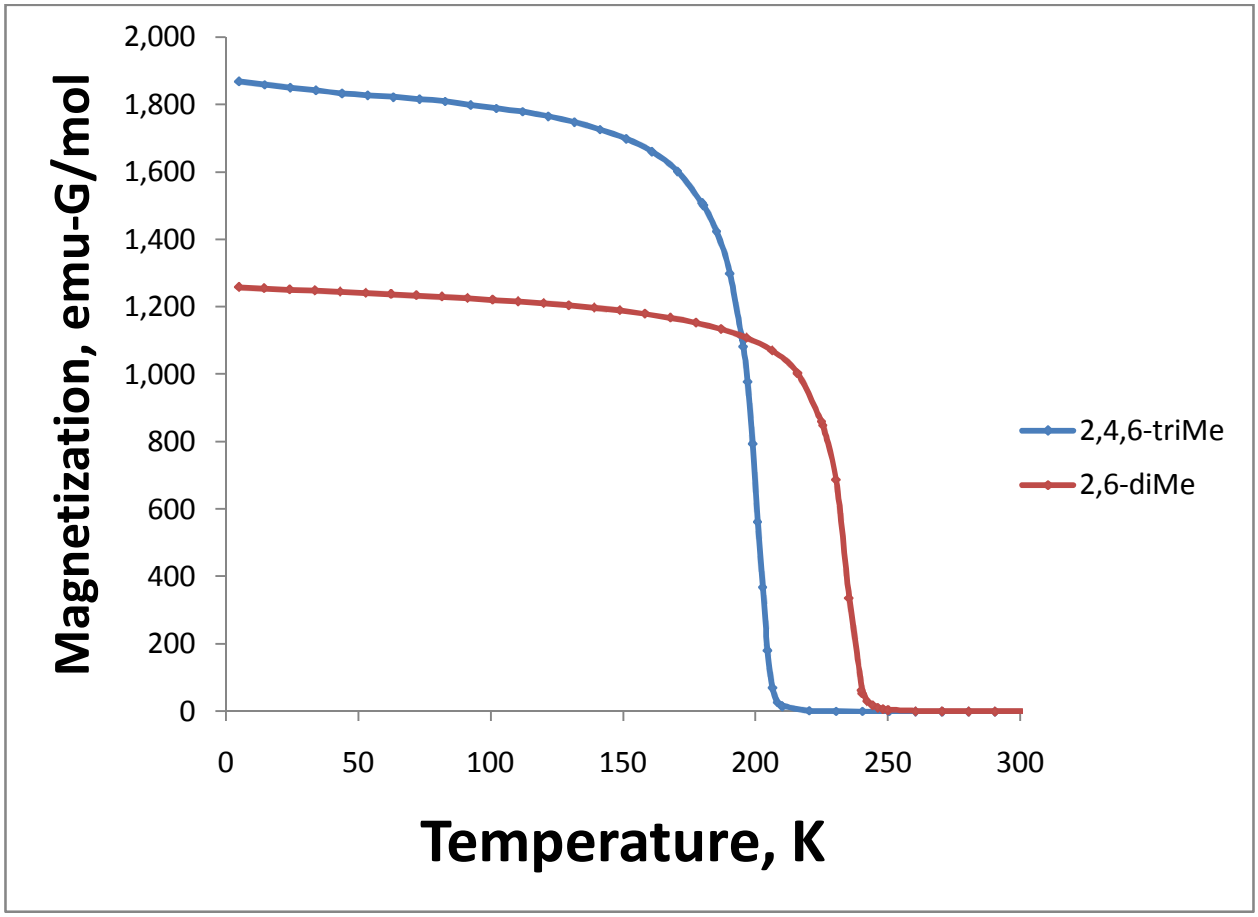

Figure 20. M vs T plot comparing the 2,6-diMePTCE and 2,4,6-triMePTCE magnets.

4.2.6 $V[Me_5PTCE]_2 \cdot 0.35CH_2Cl_2$

The last acceptor synthesized for this project contained a phenyl ring fully substituted with methyl groups, and the results were expected, yet interesting. The magnet made with the pentamethyl acceptor turned out to produce the lowest T_c for a methyl-substituted phenyl tricyanoethylene (160 K). Although this acceptor contains methyl groups in the 2 and 6 positions, the most likely reason for this acceptor giving the lowest T_c is that the five donating methyl groups caused the LUMO to rise higher in energy than in any of the other PTCE

molecules (as seen in the DFT and electrochemistry), giving a significantly less favorable orbital lineup between the acceptor LUMO and the 3d orbitals of the metal.

Table 6. T_cs of the $V[Me_xPTCE]_x$ magnets

Acceptor	T_c
2-MePTCE	244 K
3-MePTCE	200 K
4-MePTCE	182 K
2,6-diMePTCE	241 K
2,4,6-triMePTCE	209 K
Me_5PTCE	159 K

4.2.7 T_c Degradation

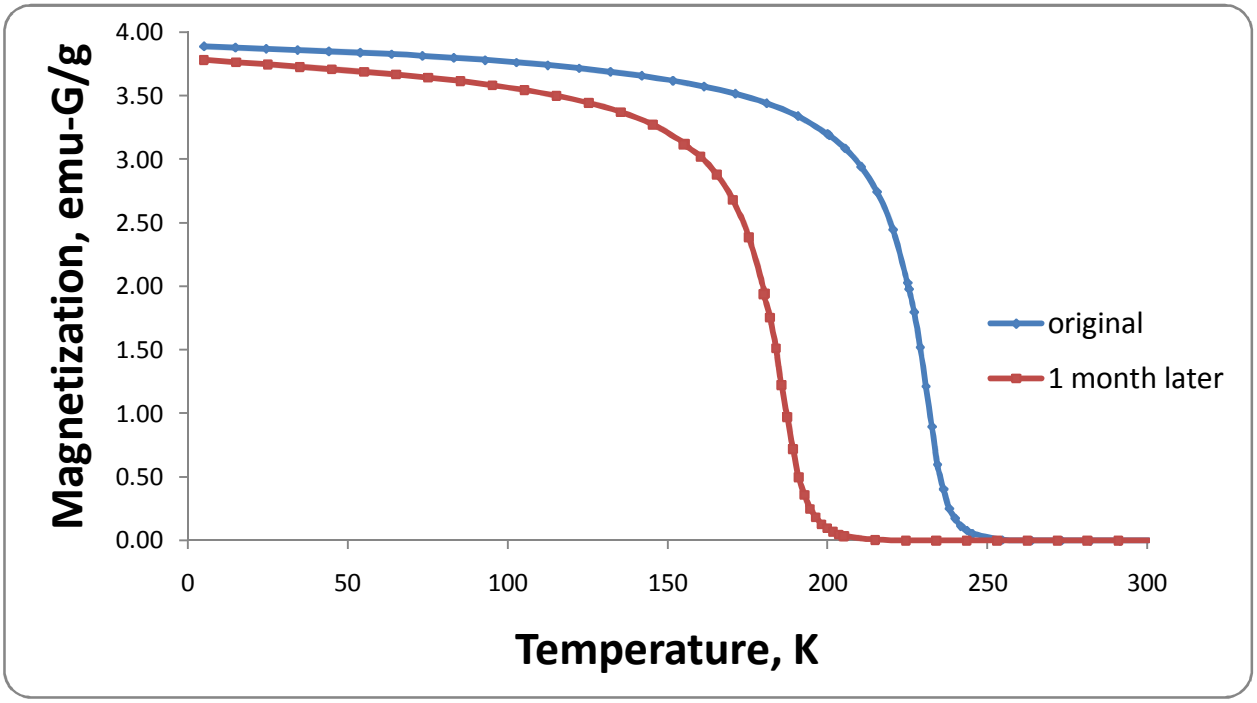

Figure 21. M vs. T plot of 2 methyl PTCE based magnet (a) upon synthesis, and (b) 33 days later. T_c decreased from 244 K to 198 K.

$V[TCNE]_2$ based magnets degrade over time, and this is also true for PTCE-based magnets. Samples prepared for magnetic measurements in this project were sealed under vacuum, so it was possible to re-measure samples to determine the extent to which their individual T_cs degrade. When M vs. T data was obtained for the 2-methyl magnet 33 days after synthesis, the T_c of the sample had decreased from 245 K to 198 K. This decrease in ordering temperature is possibly a result of thermodynamics; the initial product of the synthesis is most likely dominated by kinetics, but over time, the thermodynamically stable product begins to form and solvent molecules trapped in the structure begin to react with the vanadium ions, possibly forming V-Cl bonds. There is currently no evidence to support this however, and a detailed analysis of the aged magnet will be required to determine exactly why the T_cs are decreasing over time. In addition to magnetic measurements, infrared spectroscopy could be utilized and the spectra of the fresh sample and the aged sample could be compared to find the formation of new bonds.

4.3 M vs. H Measurements

4.3.1 Results and Discussion

Experiments measuring the magnetization of the samples as a function of applied field at 5 K were conducted to determine whether the magnets in this project exhibited any appreciable hysteresis. Magnets synthesized from all six acceptors displayed no measurable coercivities or remanences (anhysteretic behavior), which is indicative of magnets that are easily demagnetized and retain very little to no magnetization when the applied field is removed. This behavior differs only slightly from the fluorinated analogs, which typically display coercivities between 1 and 5 G, which is still considered to be negligible. The lack of any significant hysteresis in these magnets is due to the vanadium's lack of contribution of orbital angular momentum to the overall magnetic moment. The unpaired electrons on vanadium are located in the t_{2g} orbitals (d_{xy}, d_{xz}, and d_{yz}), and because all three orbitals contain electrons with the same spin, the orbital angular momentum is quenched and no anisotropy arises, which is responsible for hysteresis. M vs. H measurements were also run on aged samples as a part of the time dependent studies. The aged samples showed only slightly higher coercivites (~2 G), but the difference in coercivities suggest that the vanadiums in the solid are undergoing some reaction within the network. Again, a detailed analysis of the infrared spectrum for the aged sample must take place in order to confirm speculation involving the aged samples.

Table 7. Saturation magnetization values. * Previous work.

Magnet	T_c (K)	M_{sat} (emu-G/mol)
H_5PTCE*	215	5060
2-MePTCE	244	4080
3-MePTCE	200	6260
4-MePTCE	182	5420
2,6-diMePTCE	241	3750
2,4,6-triMePTCE	209	5130
Me_5PTCE	159	4290

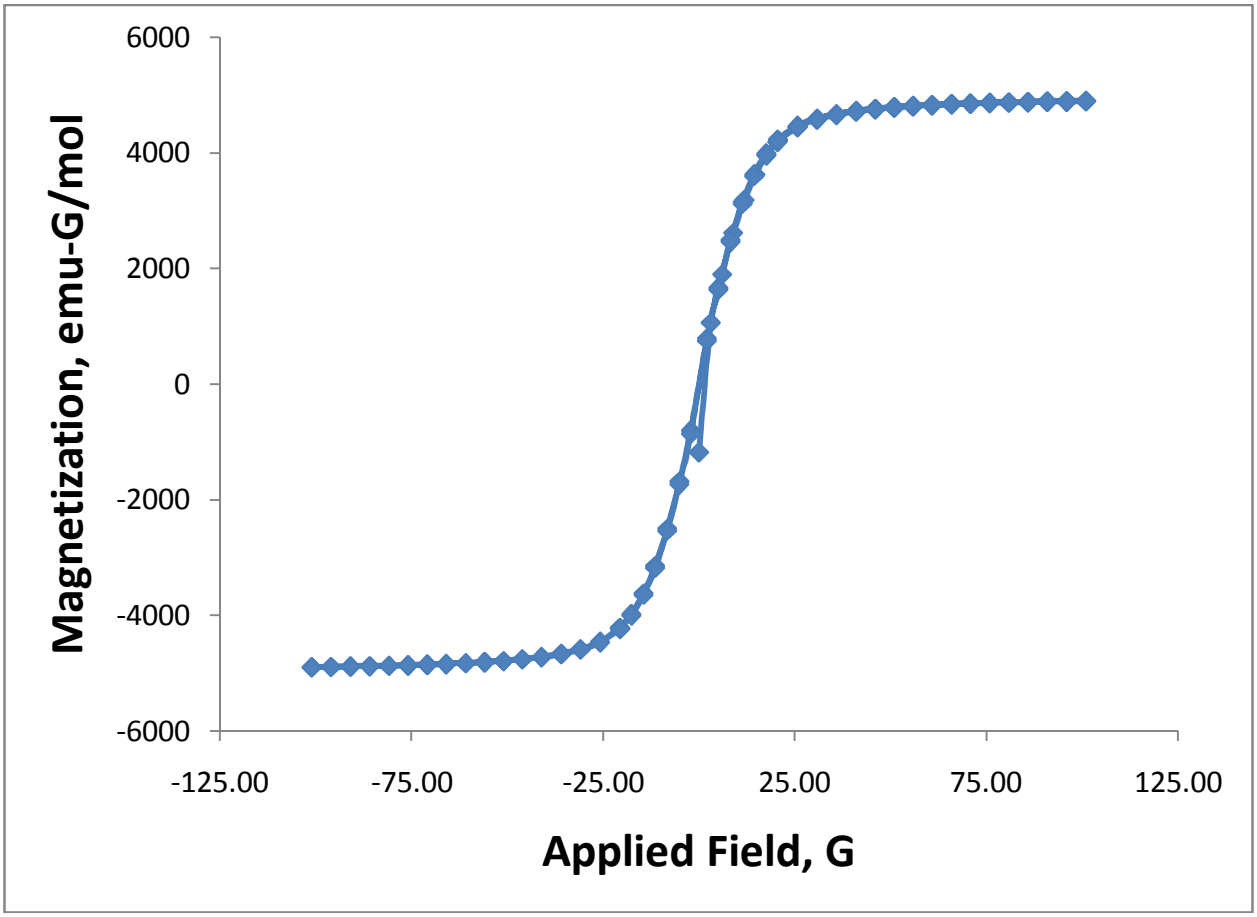

Figure 22. M vs. H plot for the 4 methyl PTCE based magnet. All magnets exhibited anhysteretic behavior.

4.4 Electrochemistry Correlation

Cyclic voltammetry experiments were performed in an attempt to correlate the T_c's of the synthesized magnets with the ease with which the individual acceptors could be reduced. All synthesized acceptors show one-electron reversibility with reduction potentials between -0.4 V and -0.6 V. However, just as with the fluoro series, there is little correlation between the T_c and reduction potentials of the acceptors. The pentamethyl acceptor turned out to be the hardest acceptor to reduce, which was expected due to the number of methyls on the ring; however, the 3-Me acceptor was the easiest to reduce, even though the 2-Me and 2,6-diMe acceptors produced higher T_c's. Some of the more unusual results of the electrochemistry come from a comparison of methyl and fluoro acceptors, particularly those substituted in the the 2 and 4 position. The 2-methyl and 2-fluoro magnets exhibit relatively similar ordering temperatures despite showing vastly different reduction potentials (comparison between the 2-CF_3PTCE and 2-FPTCE reduction potentials and ordering temperatures also suggests an increase due to sterics, as the 2-CF_3PTCE displays the higher T_c but is harder to reduce). This is also true for the 4-methyl and 4-fluoro magnets, with the 4-methyl ordering higher of the two, despite having a more negative reduction potential. This lack of a correlation between the ease of reduction and ordering temperature with this family of acceptors strengthens the argument that the relationship between steric hindrance and electronics are a significant factor in the T_cs of PTCE-based magnets.

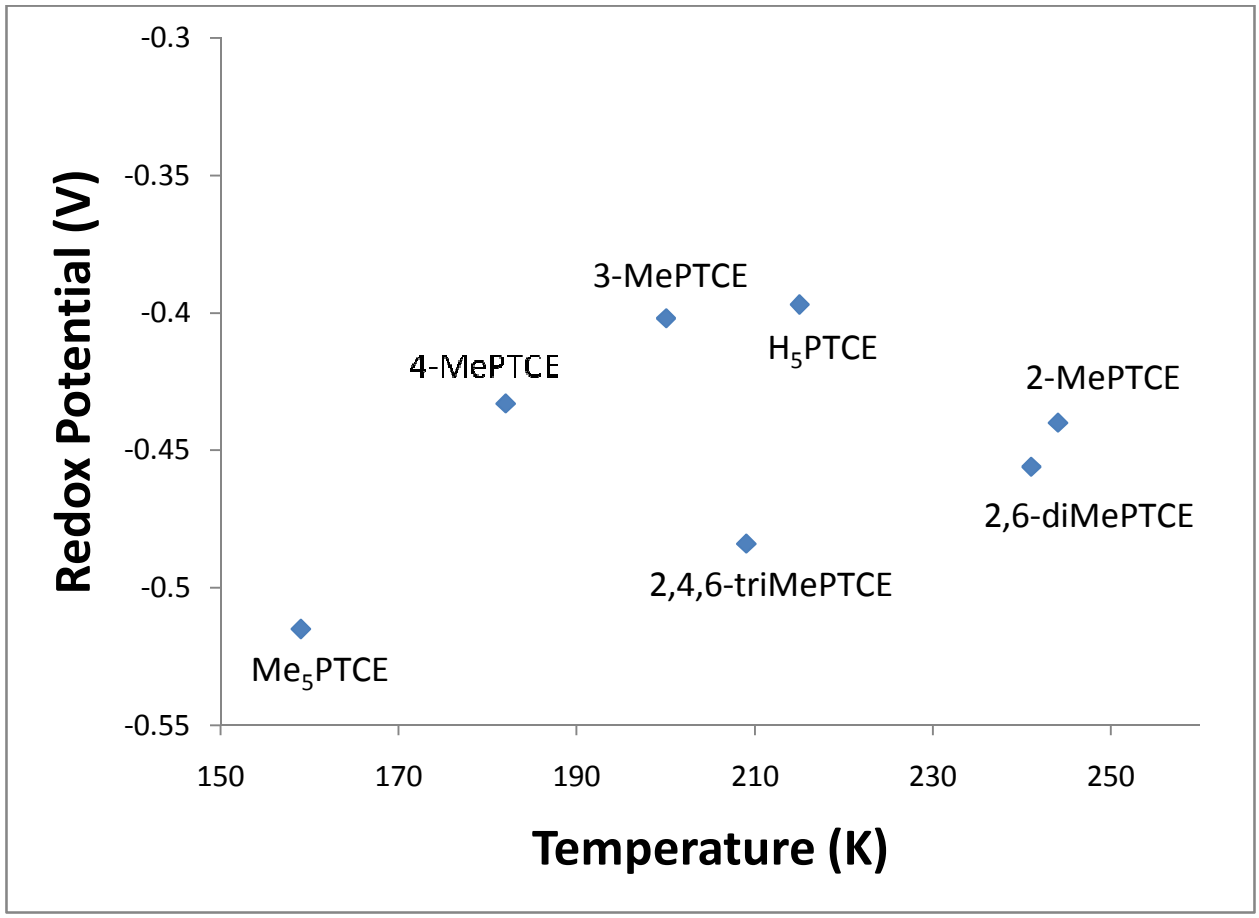

Figure 23. Plot of the acceptor $E_{1/2}$ (V) values vs T_cs of the corresponding V[Me_xPTCE] magnets.

4.5 DFT Calculations

When plotting the reduction potentials of the neutral acceptors against their respective calculated dihedral angles, there is a weak linear relationship within the data, but the main feature is the separation of the data points into two distinct groups. The unsubstituted, 4-Me, and 3-Me acceptors are grouped together within the 25-30° range and represent the higher reduction potentials (easier to reduce). The 2,6-diMe, 2,4,6-triMe, and penta-Me acceptors are grouped within the 70-80° range, and represent the lower reduction potentials (harder to reduce). Between these two groups lies the 2-Me acceptor, which exhibits a dihedral angle ~52° and a reduction potential between the two groups. These groupings suggest that the acceptors with

lower dihedral angles (H_5PTCE, 3-MePTCE and 4-MePTCE) are more easily reduced due to increased conjugation throughout the molecule.

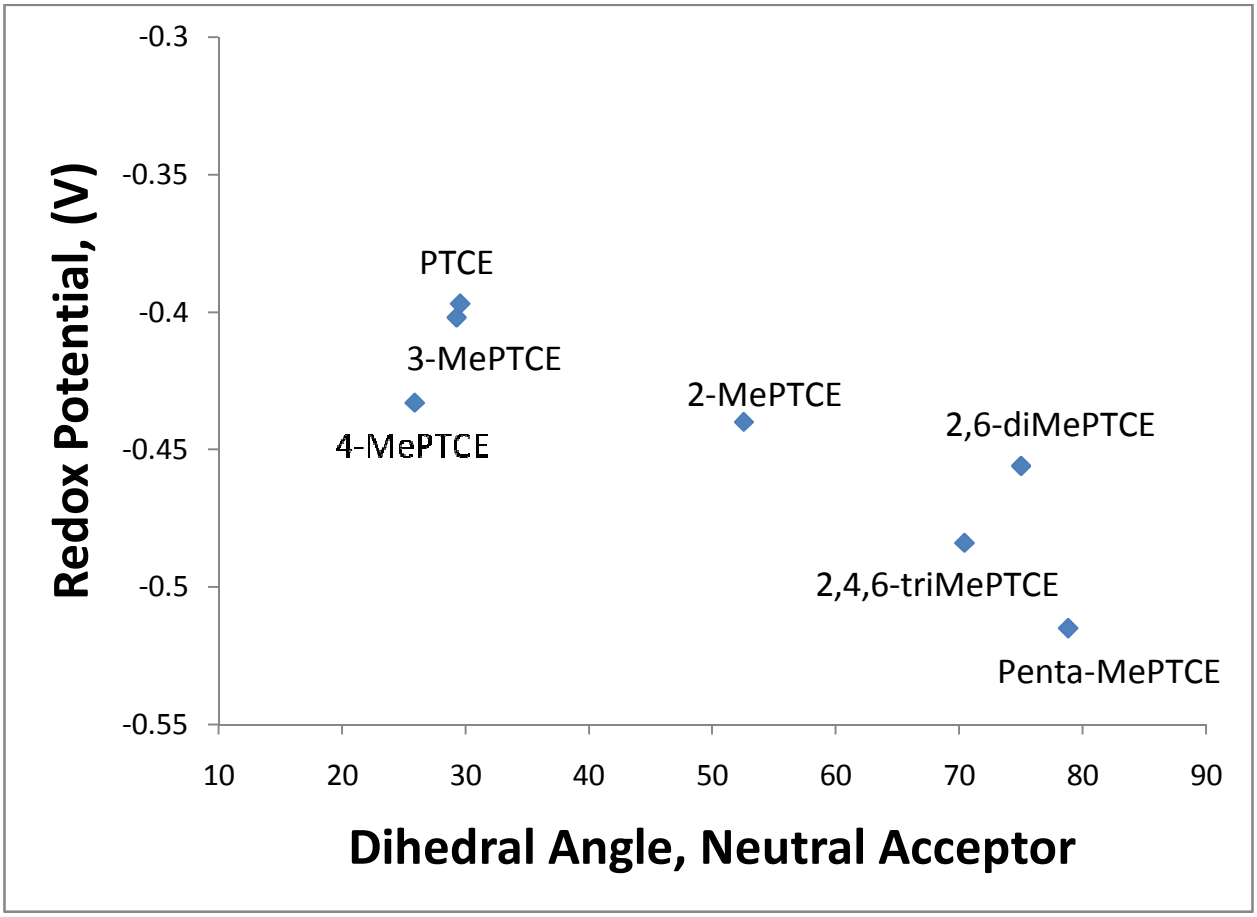

Figure 24. Plot of the acceptor $E_{1/2}$ values vs the neutral acceptor dihedral angles.

A plot of the dihedral angles in the radical anions as a function of ordering temperature provided no correlation whatsoever, as the data were again separated into groups in different regions of the graph with no apparent relation. As in the previous plot, the 2,6-diMe, 2,4,6-triMe and penta-Me anions made one group, the 3-Me, 4-Me and unsubstituted acceptors made another group, with the 2-Me lying in between them.

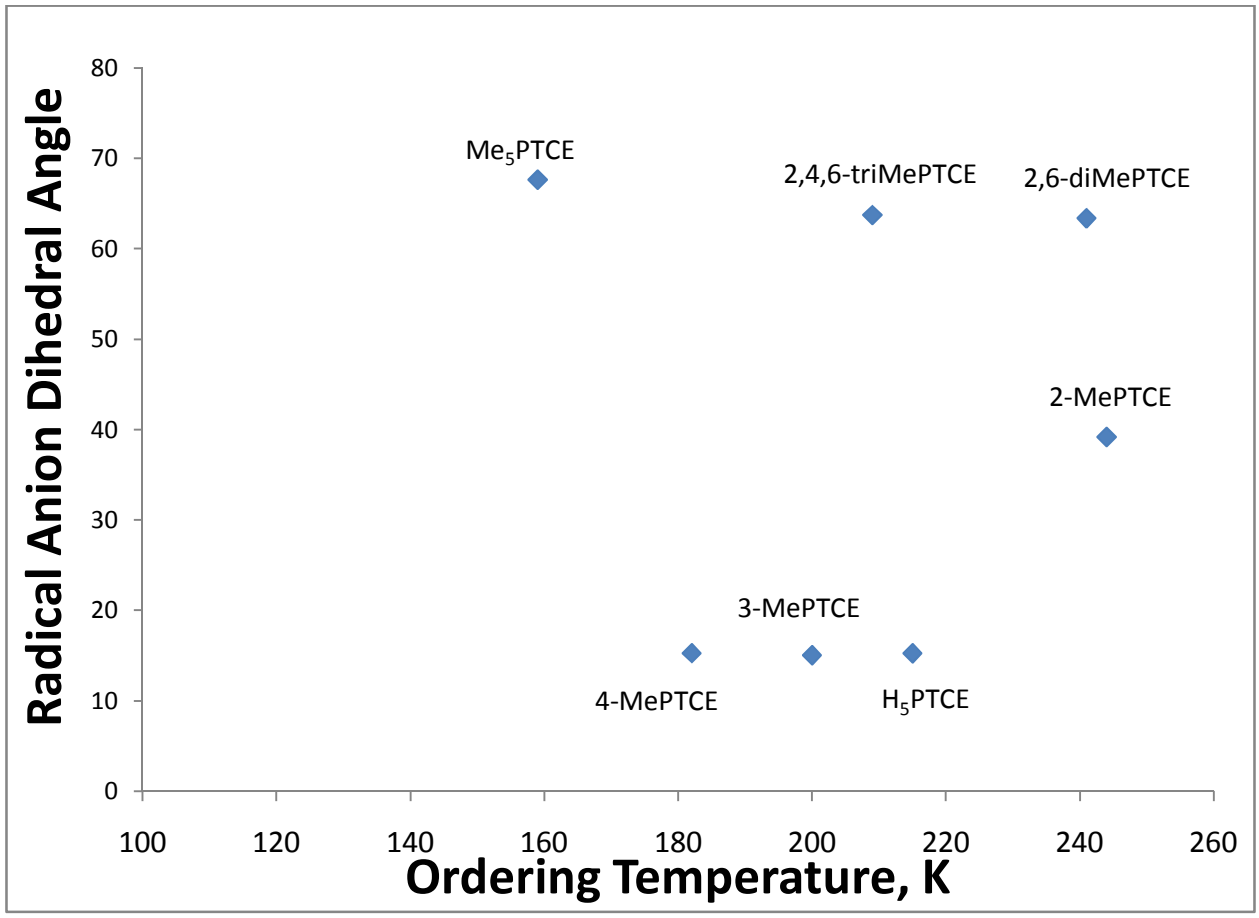

Figure 25. Plot of the acceptor radical anion dihedral angles vs the T_cs of the corresponding magnets.

The electron affinities were calculated as according to Rienstra-Firacofe and co-workers (35), where the electron affinity (EA) in our case is the energy of the optimized, neutral acceptor with the energy of the optimized, anionic form of the acceptor subtracted out. The calculated electron affinities agree reasonably with the experimentally determined redox potentials of the acceptors, forming a linear relationship when plotted against each other. Unfortunately, the electron affinities, like the reduction potentials, show no appreciable correlation with the ordering temperatures of the magnets.

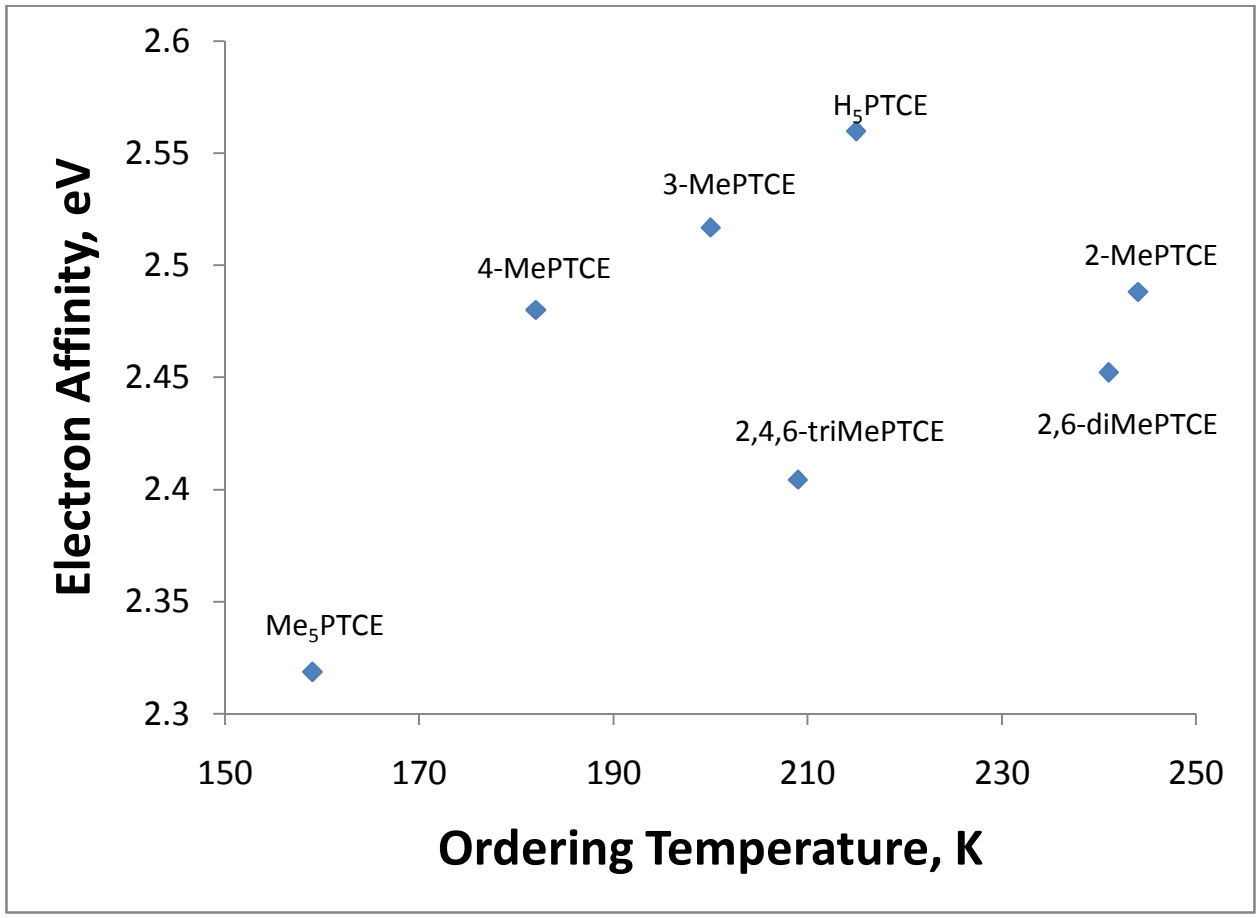

Figure 26. Plot of the acceptor electron affinities vs the T_cs of the corresponding magnets.

The final property of interest from the DFT calculations involved the Mulliken spin densities of the nitrogen atoms from the radical anions. The nitrogen spin densities were summed together for each acceptor and those quantities were plotted against the ordering temperatures of the resulting magnets with the hopes of some correlation. No linear relationship was established, but the discernable groupings helped solidify an earlier notion concerning conjugation within the molecule. The highest total nitrogen spin densities corresponded to those acceptors with ortho-substituted phenyl rings (2-Me, 2,6-diMe, 2,4,6-triMe, and pentaMe), while those without ortho substitution (3-Me, 4-Me, and unsubstituted) formed a grouping with significantly lower spin densities. This suggests that as the dihedral angle between the phenyl ring and the olefin increases (acceptors with ortho substitutions have been shown to have larger

dihedral angles than those without), more spin density is located on the nitrogen-containing olefin fragment of the molecule.

This is also supported by the spin densities of the para carbons of each acceptor. A similar grouping can be seen, only the lower angle group possesses the higher spin densities. This result, however, still fails to give a strong correlation between the acceptor molecules and the ordering temperatures of their resulting magnets; for instance, the pentaMe acceptor gives the largest nitrogen spin density (0.488) but its resulting magnet produces the lowest T_c (159 K).

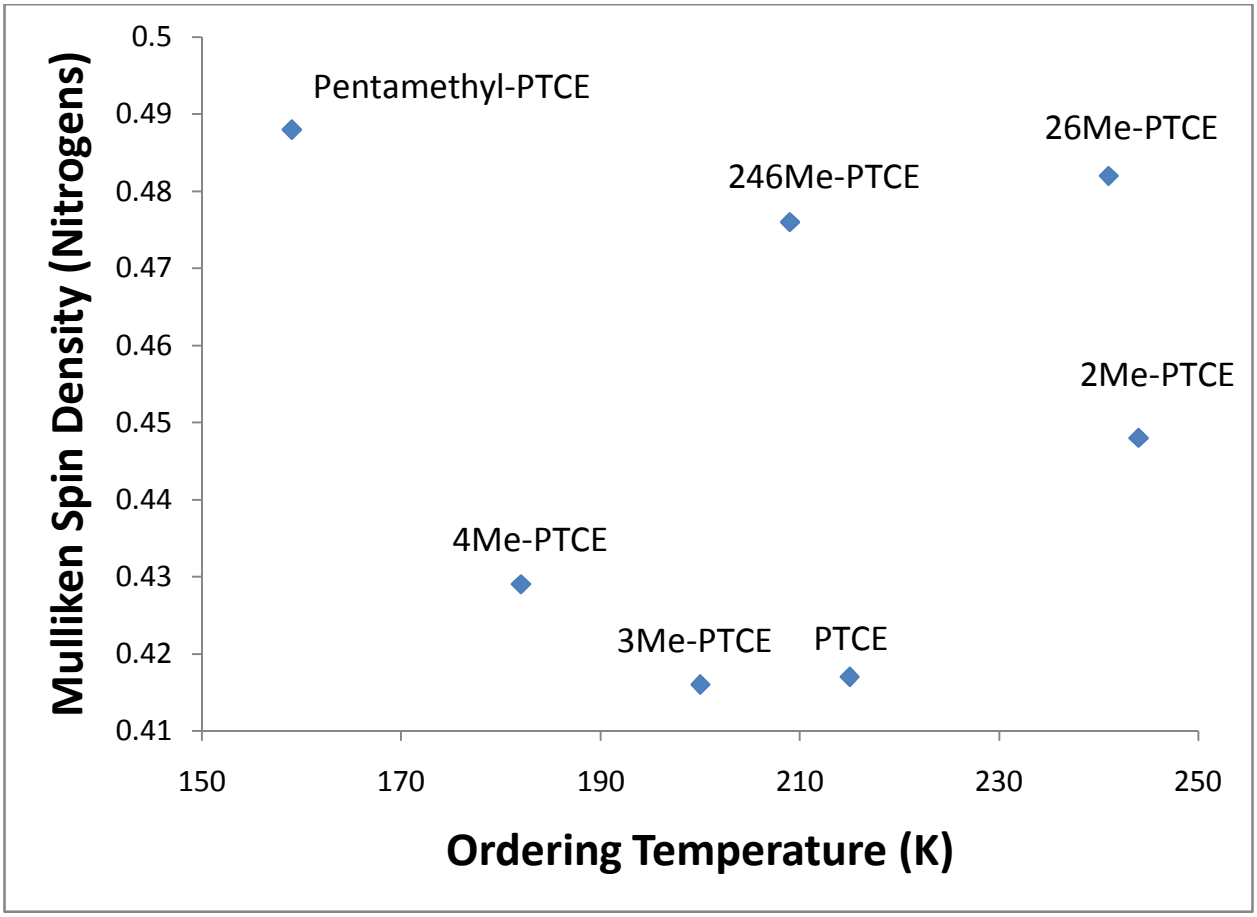

Figure 27. Plot of the calculated Mulliken Spin Densities summed over the nitrogen atoms vs the T_cs of the magnets.

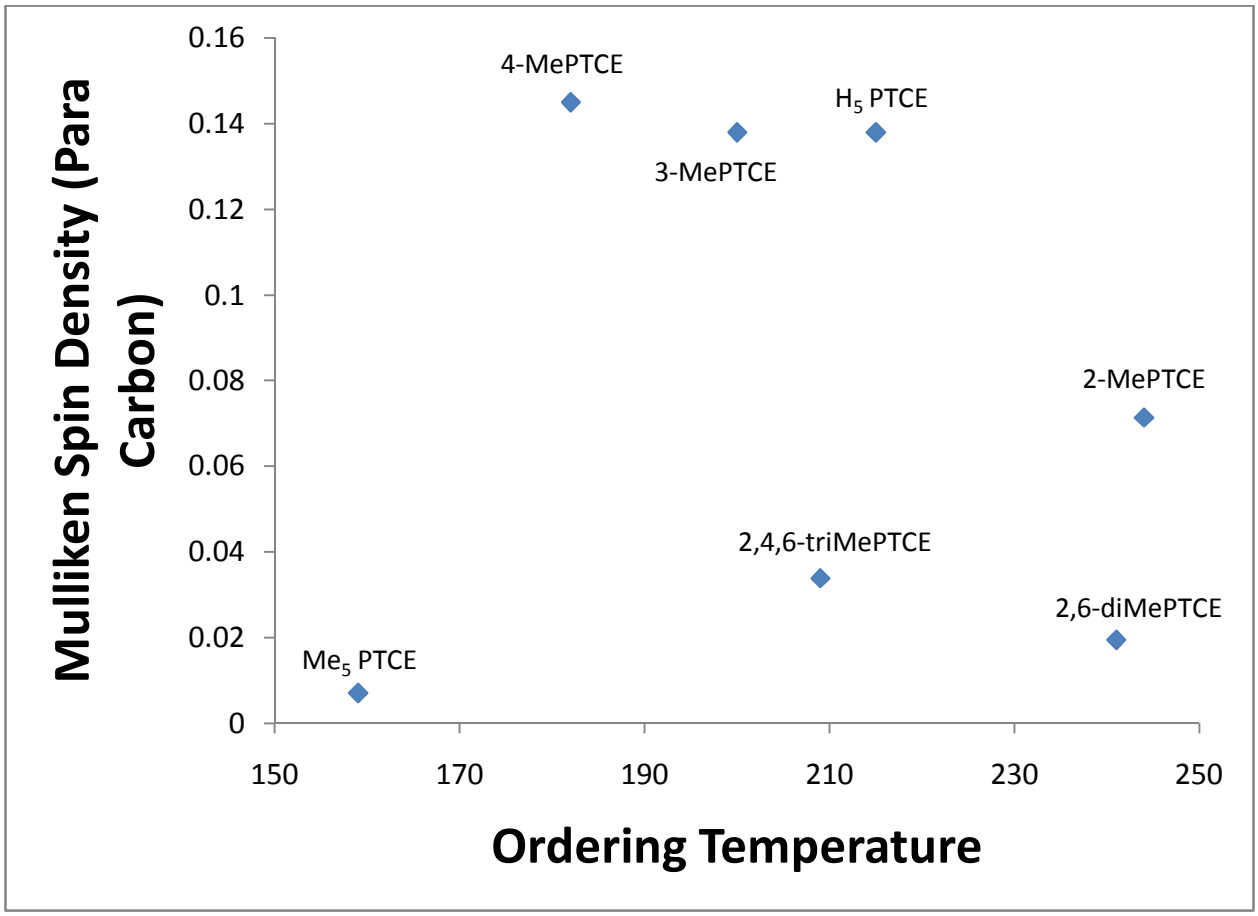

Figure 28. Plot of the calculated Mulliken Spin Densities of the para carbon atoms vs the Tcs of the magnets.

The DFT calculations performed for this project have provided valuable information, especially concerning acceptor structure. The calculations suggest that the dihedral angle in the acceptors does play a significant role in the ordering temperature because the 2-MePTCE and 2,6-diMePTCE both exhibit higher angles (>45°) and order above the H_5PTCE despite containing donating groups. The lack of a strong correlation between the three different sets of DFT data and the magnetic data suggests that both electronic and structural properties are responsible in determining ordering temperatures within the magnetic solids. With enough data from more acceptors, one may eventually be able to generate an equation for calculating T_c that accurately factors in experimentally determined and calculated properties of the acceptors such as reduction potentials, dihedral angles and orbital energies.

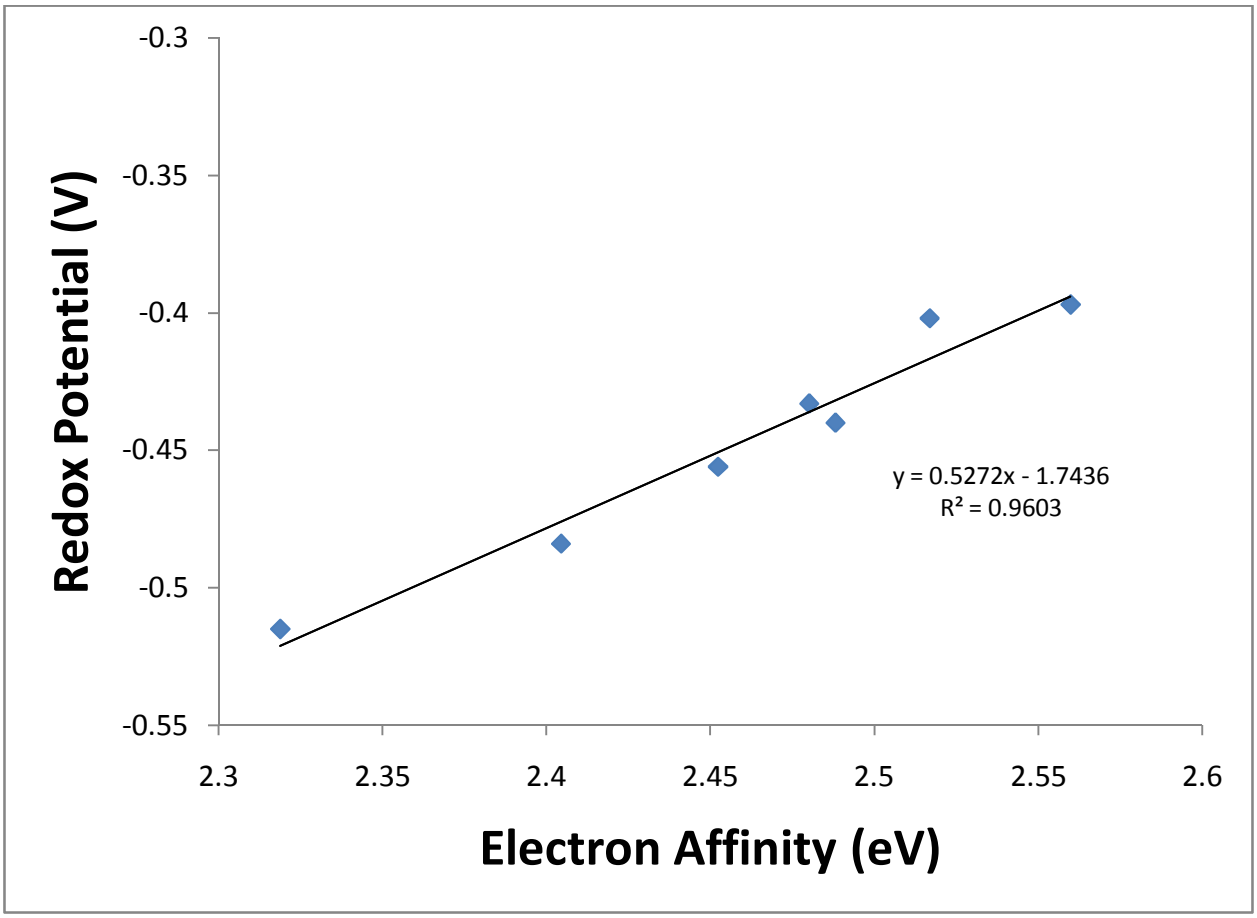

Figure 29. Plot of the acceptor redox potentials vs the acceptor electron affinities.

5. Conclusions

5.1 What we learned

The family of acceptors studied in this project not only reaffirms the versatility of PTCE as a suitable building block for studying the V[acceptor] system, it has led to a better understanding of the electronic and steric effects of the ring that influence the ordering temperatures of these magnetic solids. While it is apparent that substituting electron-withdrawing groups around the ring generally lead to higher T_c values than analogous acceptors with electron-donating groups, comparisons between magnets containing donating and withdrawing groups around the ring have shown that steric hindrance from withdrawing or

donating groups can help increase ordering temperature, as well as the detrimental effects of electron donating groups substituted on the 4 position on the ring.

The magnetic data obtained from this particular family of magnets have helped to increase our library of molecule-based magnets by providing acceptors with substituents that can be compared sterically to similar acceptors with different electronic properties. The $–CH_3$ and $–CF_3$ groups are similar in size, yet display drastically different electronic properties ($-CH_3$ is weakly donating, $-CF_3$ is strongly withdrawing). Comparing the 2-MePTCE (244 K) and 2-CF_3PTCE (259 K) magnets has shown that steric hindrance (specifically, a larger dihedral angle between the phenyl and olefin moieties) can increase T_c relative to the H_5PTCE magnet. The 3-MePTCE (200 K) and 3-CF_3PTCE (220 K) magnets support the hypothesis that withdrawing groups increase T_c and donating groups decrease T_c relative to H_5PTCE. This trend is also seen in the 4-MePTCE (182 K) and 4-CF_3PTCE (230 K) magnets, and when compared to the 4-FPTCE magnet (159 K), this suggests that if a substituent is capable of electron donation, it should not be used in the 4 position if higher ordering temperatures are desired.

Table 8. Summary of magnetic and acceptor properties for $V[Me_xPTCE]_x$ magnets. * Previous work.

Acceptor/Magnet	T_c (K)	M_{sat} (emu-G/mol)	Redox Potential (V)	Electron Affinity (eV)	Dihedral Angle, anion (°)
H_5PTCE*	215	5060	-0.397	2.56	15.29
2-MePTCE	244	4080	-0.440	2.49	39.19
3-MePTCE	200	6260	-0.402	2.52	15.08
4-MePTCE	182	5420	-0.433	2.48	15.30
2,6-diMePTCE	241	3750	-0.456	2.45	63.37
2,4,6-triMePTCE	209	5130	-0.484	2.40	63.71
Me_5PTCE	159	4290	-0.515	2.32	67.61

5.2 Future Plans

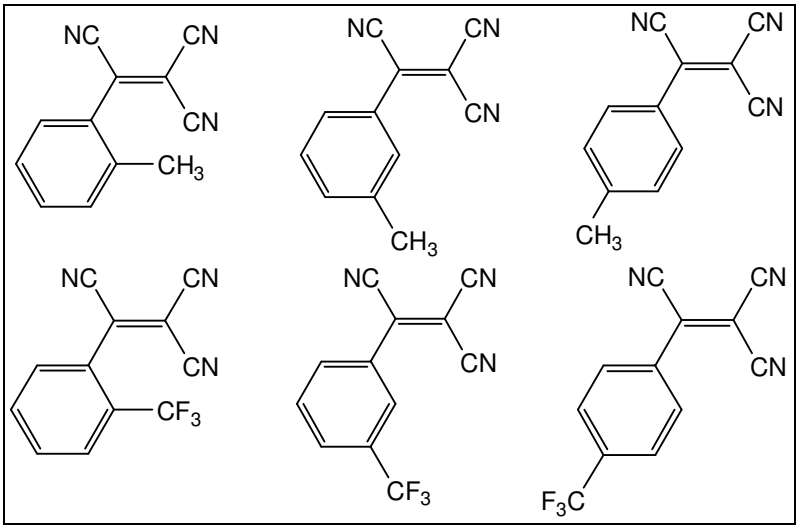

Figure 30. Isostructural PTCE acceptors containing methyl and trifluoromethyl groups.

Preliminary studies have been done concerning n-CF_3PTCE-based magnets (specifically, all three monosubstituted analogues), but for meaningful correlations and conclusions to be

obtained, more isostructural acceptors of both $-CH_3$ and $-CF_3$ containing molecules will have to be synthesized so the properties of the resulting magnets can be analyzed and compared. Examples of new acceptors could be the 2,6-diCF_3PTCE, 2,4,6-triCF_3PTCE, and pentaCF_3PTCE molecules to compare to the acceptors involved with this study. Since the benzaldehydes corresponding to these acceptors are not commercially available, they can be synthesized from the corresponding phenols through oxidation (36).

In addition to synthesizing more isostructural acceptors (such as 2,6-diCF_3PTCE and 2,4,6-triCF_3PTCE) for the magnet synthesis, an in-depth solvent study could also be beneficial to maximizing ordering temperatures. As discussed earlier, the T_c of magnets related to the $V[TCNE]_x$ system can vary with solvent. However, there is not any evidence in the literature pertaining to the affects of multi-solvent systems on T_c. For instance, using acetonitrile for the reaction between $V(CO)_6$ and TCNE has proven to be detrimental to T_c. However, using smaller amounts of acetonitrile together with one of the better solvents for TCNE (i.e. dichloromethane) could be beneficial if the acetonitrile coordinates any of the open V^{2+} sites that may exist after TCNE coordinates.

Experimental Section

The following procedure describes the synthesis of electron-poor acceptors that have one of the cyano groups of TCNE replaced by a phenyl group with methyl substituents around the ring. The 2-methyl acceptor synthesis is based loosely on literature procedures (32) and is described in detail here; the synthesis for the 3-methyl, 4-methyl, 2,6-dimethyl, 2,4,6-trimethyl, and pentamethyl acceptors follow the same procedure with minor alterations (noted). All reagents were used as received, except for the following: the dichloromethane used in the

magnet synthesis was distilled from P_2O_5, and the $V(CO)_6$ was prepared, using a procedure from the literature, from $[Et_4N]^+ [V(CO)_6]^-$ (37).

2-(2-methylphenyl)-1,1,2-tricyanoethylene

2-(2-methylphenyl)-1,1-dicyanoethylene (**1**):

To a solution of 2-methylbenzaldehyde (3.573 g, 0.0297 mol) and malononitrile (2.13 g, 0.0322 mol) in ethanol (80 mL) was added one drop of piperidine. After stirring for 10 minutes, the stir bar was removed, and the beaker was covered with parafilm and set aside for the night. White crystals began to form within two hours of the completion of the reaction. The white crystals were collected the following day, and washed with ethanol (95%) to afford 2.43 g of 1 (49%). IR (KBr): ν(CN), 2232 cm^{-1} and 2177 cm^{-1}. ^1H NMR (400 MHz, $CDCl_3$) δ 8.06 (m, 1H), 7.46 (m, 2H), 7.31 (m, 2H), 2.41 (s, 3H).

2-(2-methylphenyl)-1,1,2-tricyanoethane (**2**):

One equivalent of **1** (1.20 g, 0.00713 mol) was dissolved in 100 mL of ethanol (100%) in a 600 mL beaker with minimal heating. To this solution was added approximately 2 equivalents of KCN (1.04 g, 0.0160 mol) dissolved in ice cold water, along with more ice cold water in order to fill to 400 mL. The reaction solution was immediately placed in an ethanol/H_2O ice bath at ~ -7°C to prevent the product from polymerizing. The reaction was allowed to stir for approximately 1 hour, after which concentrated HCl was added to neutralize the solution. Upon adding the HCl, a white solid began to precipitate from the solution. After obtaining a pH around 6, the reaction was allowed to stir for 10 minutes, and the reaction beaker was covered with parafilm containing holes to release gaseous HCN. The beaker was then placed in the refrigerator overnight to allow the product to continue forming. The crystals were collected and

washed with cold H_2O the next day, and were then dried under vacuum for approximately 4 hours, weighed, and stored. 1.182 g of **2** were collected for a yield of 85%. IR (KBr): ν(CN), 2249 cm^{-1} and 2261 cm^{-1}. ^1H NMR (400 MHz, $CDCl_3$) δ 7.59 (m, 2H), 7.37 (m, 1H), 7.27 (m, 1H), 4.69 (d, 1H), 4.18 (d, 1H), 2.41 (s, 3H) ppm versus TMS.

2-(2-methylphenyl)-1,1,2-tricyanoethylene:

One equivalent of **2** (1.10 g, 0.00564 mol) was added to a 250 ml round-bottom flask along with 40 ml of diethyl ether. An excess of n-chlorosuccinimide (NCS) was then added with 80 ml of H_2O to the round-bottom, and the 2-layered solution was then stirred until all of the NCS dissolved (~30 minutes). The organic layer turned light yellow in color as more NCS dissolved. After stirring, the aqueous layer was removed using a separatory funnel, and the organic layer was washed 3 times with H_2O and dried with anhydrous Na_2SO_4. The ether was then removed by rotoevaporation, leaving yellow oil (a result of residual H_2O) in the bottom of the flask which was dried under vacuum overnight. The resulting solid (yellow, stained with purple) was dissolved with dichloromethane and loaded onto a silica gel flash column with dichloromethane as the mobile phase. The desired product was the first compound to elute off of the column. The product was dried under vacuum, forming a pale yellow solid that was weighed and stored in the glovebox. Yield: 0.791 g (73%). Mp: 118.2-118.8 °C. IR (KBr): ν(CN), 2240 cm^{-1} and 2247 cm^{-1}. ^1H NMR (400 MHz, $CDCl_3$) δ 7.52 (m, 2H), 7.37 (m, 2H), 2.48 (s, 3H) ppm versus TMS. HRMS-ESI (*m/z*, [M-H]-). Calcd for $C_{12}H_8N_3$: 194.2162. Found: 194.0724

2-(3-methylphenyl)-1,1,2-tricyanoethylene

3-MePTCE was synthesized using a similar procedure, using 3-methylbenzaldehyde as the starting material.

2-(3-methylphenyl)-1,1-dicyanoethylene

Yield: 2.24 g (55%). IR (KBr): ν(CN), 2230 cm^{-1} and 2195 cm^{-1}. ^1H NMR (400 MHz, $CDCl_3$) δ 7.71 (s, 1H), 7.68 (m, 2H), 7.41 (m, 2H), 2.40 (s, 3H) ppm versus TMS.

2-(3-methylphenyl)-1,1,2-tricyanoethane

Yield: 1.51 g (87%). IR (KBr): ν(CN), 2253 cm^{-1} and 2267 cm^{-1}. ^1H NMR (400 MHz, $CDCl_3$) δ 7.35 (m, 4H), 4.39 (d, 1H), 4.20 (d, 1H), 2.41 (s, 3H) ppm versus TMS.

2-(3-methylphenyl)-1,1,2-tricyanoethylene

Yield: 0.441 g (62%). Mp: 109.1-109.8 °C. IR (KBr): ν(CN), 2234 cm^{-1} and 2196 cm^{-1}. ^1H NMR (400 MHz, $CDCl_3$) δ 7.79 (m, 2H), 7.45 (m, 2H), 2.44 (s, 3H) ppm versus TMS. HRMS-ESI (*m/z*, [M-H]-). Calcd for $C_{12}H_8N_3$: 194.2162. Found: 194.0724

2-(4-methylphenyl)-1,1,2-tricyanoethylene

4-MePTCE was synthesized using a similar procedure, using 4-methylbenzaldehyde as the starting material.

2-(4-methylphenyl)-1,1-dicyanoethylene

Yield: 3.75 g (89%). IR (KBr): ν(CN), 2229 cm^{-1} and 2202 cm^{-1}. ^1H NMR (400 MHz, $CDCl_3$) δ 7.78 (d, 2H), 7.30 (d, 2H), 2.42 (s, 3H) ppm versus TMS*.

2-(4-methylphenyl)-1,1,2-tricyanoethane

Yield: 1.98 g (88%). IR (KBr): ν(CN), 2249 cm^{-1} and 2259 cm^{-1}. ^1H NMR (400 MHz, $CDCl_3$) δ 7.35 (d, 2H), 7.29 (d, 2H), 4.38 (d, 1H), 4.17 (d, 1H), 2.38 (s, 3H) ppm versus TMS.

2-(4-methylphenyl)-1,1,2-tricyanoethylene

Yield: 0.394 g (28%). Mp: 120.5-121.0 °C. IR (KBr): ν(CN), 2235 cm^{-1} and 2198 cm^{-1}. ^1H NMR (400 MHz, $CDCl_3$) δ 7.92 (d, 2H), 7.38 (d, 2H), 2.47 (s, 3H) ppm versus TMS. HRMS-ESI (*m/z*, [M-H]-). Calcd for $C_{12}H_8N_3$: 194.2162. Found: 194.0722.

2-(2,6-dimethylphenyl)-1,1,2-tricyanoethylene

2,6-diMePTCE was synthesized using a similar procedure, using 2,6-dimethylbenzaldehyde as the starting material.

2-(2,6-dimethylphenyl)-1,1-dicyanoethylene

Yield: 1.76 g (43%). IR (KBr): ν(CN), 2237 cm^{-1} and 2201 cm^{-1}. ^1H NMR (400 MHz, $CDCl_3$) δ 8.13 (s, 1H), 7.28 (m, 2H), 7.16 (m, 1H), 2.55 (s, 6H) ppm versus TMS.

2-(2,6-dimethylphenyl)-1,1,2-tricyanoethane

Yield: 2.01 g (87%). IR (KBr): ν(CN), 2246 cm^{-1} and 2269 cm^{-1}. ^1H NMR (400 MHz, $CDCl_3$) δ 7.27 (m, 2H), 7.15 (m, 1H), 4.92 (d, 1H), 4.38 (d, 1H), 2.54 (s, 6H) ppm versus TMS.

2-(2,6-dimethylphenyl)-1,1,2-tricyanoethylene

Yield: 1.23 g (62%). Mp: 116.8-117.5 °C. IR (KBr): ν(CN), 2240 cm^{-1} and 2242 cm^{-1}. ^1H NMR (400 MHz, $CDCl_3$) δ 7.34 (m, 1H), 7.17 (d, 2H), 2.33 (s, 6H) ppm versus TMS. HRMS-ESI (*m/z*, [M-H]-). Calcd for $C_{13}H_{10}N_3$: 208.243. Found: 208.088

2-(2,4,6-trimethylphenyl)-1,1,2-tricyanoethylene

2,4,6-triMePTCE was synthesized using a similar procedure, using 2,4,6-trimethylbenzaldehyde as the starting material.

2-(2,4,6-trimethylphenyl)-1,1-dicyanoethylene

Yield: 3.02 (52%). IR (KBr): ν(CN), 2239 cm^{-1} and 2216 cm^{-1}. ^1H NMR (400 MHz, $CDCl_3$) δ 8.10 (s, 1H), 6.92 (m, 2H), 2.28 (s, 3H), 2.26 (s, 6H) ppm versus TMS.

2-(2,4,6-trimethylphenyl)-1,1,2-tricyanoethane

Yield: 2.85 g (85%). IR (KBr): ν(CN), 2255 cm^{-1} and 2272 cm^{-1}. ^1H NMR (400 MHz, $CDCl_3$) δ 6.94 (m, 2H), 4.86 (d, 1H), 4.34 (d, 1H), 2.46 (s, 6H), 2.26 (s, 3H) ppm versus TMS.

2-(2,4,6-trimethylphenyl)-1,1,2-tricyanoethylene

Yield: 0.654 g (33%). Mp: 108.2-108.9 °C. IR (KBr): ν(CN), 2238 cm^{-1} and 2245 cm^{-1}. ^1H NMR (400 MHz, $CDCl_3$) δ 6.99 (s, 2H), 2.32 (s, 3H), 2.31 (s, 6H) ppm versus TMS. HRMS-ESI (*m/z*, [M-H]-). Calcd for $C_{14}H_{12}N_3$: 222.270. Found: 222.104

2-(pentamethylphenyl)-1,1,2-tricyanoethylene

Penta-MePTCE was synthesized using a similar procedure, using pentamethylbenzaldehyde as the starting material.

2-(pentamethylphenyl)-1,1-dicyanoethylene

Yield: 2.06 g (63%). IR (KBr): ν(CN), 2235 cm^{-1} and 2203 cm^{-1}. ^1H NMR (400 MHz, $CDCl_3$) δ 8.23 (s, 1H), 2.24 (s, 6H), 2.19 (s, 9H) ppm versus TMS.

2-(pentamethylphenyl)-1,1,2-tricyanoethane

Yield: 1.44 g (78%). IR (KBr): ν(CN), 2242 cm^{-1} and 2264 cm^{-1}. ^1H NMR (400 MHz, $CDCl_3$) δ 5.08 (d, 1H), 4.35 (d, 1H), 2.26 (s, 3H), 2.24 (s, 12H) ppm versus TMS.

2-(pentamethylphenyl)-1,1,2-tricyanoethylene

Yield: 0.396 g (41%). Mp: compound burned at 180 °C. IR (KBr): ν(CN), 2239 cm^{-1} and 2249 cm^{-1}. ^1H NMR (400 MHz, $CDCl_3$) δ 2.27 (s, 3H), 2.23 (s, 12H) ppm versus TMS. HRMS-ESI (*m/z*, [M]). Calcd for $C_{16}H_{15}N_3$: 249.316. Found: 249.127

V[2-MePTCE]$_2$:

All reactions involving the synthesis of magnets were carried out in a Vacuum Atmospheres Glovebox with N_2 (ultra-high purity) as the atmosphere. Approximately 2.5 equivalents of the acceptor (2-methyl-PTCE, 60.0 mg) were dissolved in roughly 1.0 ml of dichloromethane in a 50 ml round-bottom flask and left to stir (solution was yellow in color). 1 equivalent of $V(CO)_6$ (25.0 mg) was dissolved in 1.5 ml of dichloromethane in a vial (solution was also yellow in color), and immediately added to the acceptor in solution. The resulting solution turned dark almost immediately, giving a black-green color that eventually turned black. The reaction was allowed to stir for 30 minutes, after which the dark suspension was passed through a medium frit. The black solid left in the frit was washed with dichloromethane until the filtrate ran clear, dried under vacuum for an hour, and then weighed and stored in a vial. Yield: 47.2 mg (89%). IR (KBr): ν(CN), 2215 cm^{-1} and 2119 cm^{-1}. Anal. Calc. for $C_{24}H_{14}N_6V_1 \cdot 0.32CH_2Cl_2$: C, 62.88; H, 3.18; N, 18.09. Found: C, 62.91; H, 3.63; N, 17.70.

All other magnets were synthesized using a procedure similar to the one used to synthesize V[2-MePTCE]$_2$.

V[3-MePTCE]$_{2.6}$

Yield: 48.1 mg (90.5%). IR (KBr): ν(CN), 2207 cm^{-1} and 2116 cm^{-1}. Anal. Calc. for $C_{31.2}H_{18.2}N_{7.8}V_1 \cdot 0.08CH_2Cl_2$: C, 67.73; H, 3.32; N, 19.75. Found: C, 67.09; H, 3.3; N, 19.51.

V[4-MePTCE]$_2$

Yield: 44.3 mg (80.7%). IR (KBr): ν(CN), 2210 cm^{-1} and 2115 cm^{-1}. *Anal.* Calc. for $C_{24}H_{14}N_6V_1 \cdot 0.55CH_2Cl_2$: C, 60.96; H, 3.14; N, 17.38. Found: C, 60.97; H, 2.95; N, 18.37.

V[2,6-diMePTCE]$_2$

Yield: 47.7 mg (85.8%). IR (KBr): ν(CN), 2202 cm^{-1} and 2116 cm^{-1}. *Anal.* Calc. for $C_{26}H_{18}N_6V_1 \cdot 0.26CH_2Cl_2$: C, 64.70; H, 3.83; N, 17.24. Found: C, 64.68; H, 3.67; N, 17.71.

V[2,4,6-triMePTCE]$_2$

Yield: 49.3 mg (79.7%). IR (KBr): ν(CN), 2209 cm^{-1} and 2214 cm^{-1}. *Anal.* Calc. for $C_{28}H_{22}N_6V_1 \cdot 0.57CH_2Cl_2$: C, 63.33; H, 4.30; N, 15.51. Found: C, 63.32; H, 4.02; N, 16.19.

V[penta-MePTCE]$_2$

Yield: 46.0 mg (69.6%). IR (KBr): ν(CN), 2219 cm^{-1} and 2113 cm^{-1}. *Anal.* Calc. for $C_{32}H_{30}N_6V_1 \cdot 0.35CH_2Cl_2$: C, 67.07; H, 5.34; N, 14.51. Found: C, 67.08; H, 5.44; N, 14.49.

Characterization Methods

The compounds synthesized were characterized using a variety of methods. The acceptors and all steps leading to them were characterized using ^{1}H NMR spectroscopy and infrared spectroscopy. The acceptors themselves were further characterized and studied using electrochemistry, melting point determination, and molecular modeling calculations. The synthesized magnetic polymers were characterized using elemental analysis, infrared spectroscopy, and magnetic experiments which include magnetization as a function of temperature and magnetization as a function of applied field.

Magnetic Measurements

Magnetic experiments were performed on a 7 T Quantum Design MPMS SQUID magnetometer. Samples for magnetic experiments were prepared in the glovebox by pulling vacuum on the sample in a tube glass-blown from NMR tubes (SQUID tube), followed by flame sealing the tube shut with the sample remaining under vacuum. Experiments involving measurement of magnetization as a function of temperature were performed from 5 K to 300 K in a 5 G applied field. Samples were cooled in an applied field of 50 G prior to measurements. Measurements involving magnetization as a function of applied field were performed at 5 K.

Electrochemistry

The cyclic voltammetry experiments were performed using a CH Instruments model 600A potentiostat. The measurements were performed on 5 mM solutions in acetonitrile/0.1 M [n-Bu_4N][PF_6] and taken between the potential range of 0 and -700 mV at a scan rate of 100 mV/s using a polished carbon electrode with Ag/AgCl as the reference and platinum wire as the auxillary electrode.

Density Functional Theory Calculations

All calculations were performed using the B3LYP density functional with the 6-31++G** basis set within *Gaussian03*. Beginning with the optimized geometry of H_5PTCE, the neutral and anionic forms of each acceptor were calculated using geometry optimization. From each calculation the neutral and anionic energies, the Mulliken spin densities and dihedral angles were collected.

Bibliography

1. Yuan, Z.; Liu, B. *Journal of Magnetism and Magnetic Materials*. **2001**, *235*, 481.

2. Morales, M. P.; Bomati-Miguel, O.; Perez de Alejo, R.; Ruiz-Cabello, J.; Veintemillas-Verdaguer, S.; O'Grady, K. *Journal of Magnetism and Magnetic Materials.* **2003**, *266*, 102.

3. Moses, T.; Zurek, S. *Journal of Magnetism and Magnetic Materials.* **2008**, *320*, v.

4. Pilkington, M.; Gross, M.; Franz, P.; Biner, M.; Decurtins, S.; Stoeckli-Evans, H.; Neels, A. *Journal of Solid State Chemistry*. **2001**, *159*, 262.

5. Miller, J.S.; Epstein, A.J. *MRS Bulletin*. **2000**, *25(11)*.

6. Epstein, A.J. *MRS Bulletin*. **2003**, *28*, 492.

7. Ohno, H.; Matsukura, F. *Solid State Commun.* **2001**, *117*, 179.

8. Coronado, E.; Delhaes, P.; Gatteschi, D.; Miller, J.S. *Molecular Magnetism: from molecular assemblies to the devices.* Boston : Kluwer Academic, **1996**.

9. Holden, A. N.; Matthias, B. T.; Anderson, P. W.; Lewis, H. W. *Physical Review*. **1956**, *102(6)*, 1463.

10. Bozorth, R. M.; Williams, H. J.; Walsh, D. E. *Physical Review*. **1956**, *103*, 572.

11. Brown, P.J.; Chattopadhyay, T. *J. Phys.: Condens. Matter.* **1997**, *9*, 9167.

12. Meshcheryakov, V.F. *Journal of Magnetism and Magnetic Materials*. **2006**, *300*, 395.

13. Parnaste, M.; Marcellini, M.; Holmstrom, E.; Bock, N.; Fransson, J.; Eriksson, O.; Hjorvarsson, B. *J. Phys.: Condens. Matter*. **2007**, *19*, 246213.

14. Jiles, D. *Introduction to Magnetism and Magnetic Materials, 2nd Edition.* s.l. : CRC Press, **1998**.

15. Zhang, J.; Ensling, J.; Ksenofontov, V.; Gutlich, P.; Epstein, A.J.; Miller, J.S. *Angew. Chem. Int. Ed.* **1998**, *37*, 657.

16. Miller, J. S.; Calabrese, J.C.; Rommelmann, H.; Chittipeddi, S.R.; Zhang, J.H.; Reiff, W.M.; Epstein, A.J. *Journal of the American Chemical Society*. **1987**, *109*, 769.

17. Manriquez, J. M.; Yee, G.T.; McLean, R.S.; Epstein, A.J; Miller, J.S. *Science* **1991**, *252*, 1415.

18. Garde, R.; Herrera, J.M.; Villain, F.; Verdaguer, M. *Inorganica Chimica Acta*. **2008**, *361*, 3597.

19. Turov, V. D.; Lobyntsev, E.S.; Starkov, A.V. *Powder Metallurgy and Metal Ceramics*. **1979**, *18*, 119.

20. Thorum, M. S.; Pokhodnya, K.I.; Miller, J.S. *Polyhedron.* **2006**, *25(9)*, 1927.

21. Miller, J. S.; Epstein, A.J. *Synthetic Metals*. **1993**, *56*, 3291.

22. Her, J. H.; Stephens, P.W.; Pokhodnya, K.I.; Bonner, M.; Miller, J.S. *Angew. Chem. Int. Ed.* **2007**, *46*, 1521.

23. Haskel, D.; Islam, Z.; Lang, J.; Kmety, C.; Srajer, G.; Pokhodnya, K.I.; Epstein, A.J.; Miller, J.S. *Physical Review B*. **2004**, *70*, 054422.

24. Zhou, P.; Long, S.M.; Miller, J.S.; Epstein, A.J. *Phys. Lett. A*. **1993**, *181*, 71.

25. Zhou, P.; Morin, B.G.; Miller, J.S.; Epstein, A.J. *Physical Review B.* **1993**, *48(2)*, 1325.

26. Fitzgerald, J.P.; Kaul, B.B.; Yee, G.T. *Chem. Commun.* **2000**, 49.

27. Wang, G.; Zhu, H.; Fan, J.; Slebodnick, C.; Yee, G.T. *Inorg. Chem.* **2006**, *45*, 1406.

28. Vickers, E.B.; Selby, T.D.; Thorum, M.S.; Taliaferro, M.L.; Miller, J.S. *Inorg. Chem*. **2004**, *43*, 6414.

29. Taliaferro, M. L.; Thorum, M.S.; Miller, J.S. *Angewandte Chemie* **2006**, *118*, 5452.

30. Vickers, E. B.; Selby, T.D.; Miller, J.S. *Journal of the American Chemical Society* **2004**, *126*, 3716.

31. Kaul, B. B.; Yee, G.T. *Inorganica Chimica Acta* **2001**, *326(1)*, 9.

32. Corson, B. B.; Stoughton, R.W. *Journal of the American Chemical Society* **1928**, *50*, 2825.

33. Harvey, M. D.; Pace, J.T.; Yee, G.T. *Polyhedron* **2007**, *26(9-11)*, 2037.

34. Harvey, M. D.; Crawford, T.D.; Yee, G.T. *Inorganic Chemistry* **2008**, *47(13)*, 5649.

35. Rienstra-Kiracofe, J.C.; Tschumper, G.S.; Schaefer III, H.F. *Chem. Rev.* **2002**, *102*, 231.

36. Zhang, S.; Xu, L.; Trudell, M.L. *Synthesis* **2005**, 1757.

37. Liu, X. *Inorganic Syntheses* **2004**, *34*, 96.